

SCIENTIFIC REPORTS



OPEN

Anti-cancer capacity of plasma-treated PBS: effect of chemical composition on cancer cell cytotoxicity

Wilma Van Boxem¹, Jonas Van der Paal¹, Yury Gorbanev¹, Steven Vanuytsel^{1,2}, Evelien Smits², Sylvia Dewilde³ & Annemie Bogaerts¹ 

We evaluate the anti-cancer capacity of plasma-treated PBS (pPBS), by measuring the concentrations of NO_2^- and H_2O_2 in pPBS, treated with a plasma jet, for different values of gas flow rate, gap and plasma treatment time, as well as the effect of pPBS on cancer cell cytotoxicity, for three different glioblastoma cancer cell lines, at exactly the same plasma treatment conditions. Our experiments reveal that pPBS is cytotoxic for all conditions investigated. A small variation in gap between plasma jet and liquid surface (10 mm vs 15 mm) significantly affects the chemical composition of pPBS and its anti-cancer capacity, attributed to the occurrence of discharges onto the liquid. By correlating the effect of gap, gas flow rate and plasma treatment time on the chemical composition and anti-cancer capacity of pPBS, we may conclude that H_2O_2 is a more important species for the anti-cancer capacity of pPBS than NO_2^- . We also used a 0D model, developed for plasma-liquid interactions, to elucidate the most important mechanisms for the generation of H_2O_2 and NO_2^- . Finally, we found that pPBS might be more suitable for practical applications in a clinical setting than (commonly used) plasma-activated media (PAM), because of its higher stability.

Cold atmospheric plasma (CAP) is gaining increasing interest for cancer treatment, but the underlying mechanisms are not yet fully understood^{1–3}. In general it is believed that the reactive oxygen and nitrogen species (RONS) from the plasma are responsible for oxidative damage of biomolecules present inside the cells, eventually causing cell death⁴. These RONS are formed in significant amounts in CAPs operating directly in air, but even when the discharge gas is helium or argon, as is often the case in plasma jet devices, the plasma effluent comes in contact with the surrounding air when leaving the jet device, thus also forming RONS. Moreover, the discharge gas often contains some N_2 , O_2 or H_2O admixtures, thus the RONS can also directly be formed in the plasma.

The anti-cancer capacity of CAP has been reported already for many different cancer cell lines, including breast cancer^{5,6}, lung cancer^{7–9}, leukaemia¹⁰, pancreatic cancer¹¹, liver cancer^{12–14}, glioblastoma^{15–18}, cervical cancer¹⁹, melanoma^{18–23}, etc. Furthermore, CAP has been demonstrated to act selectively towards cancer cells, while leaving normal cells undamaged^{1–4}. This selectivity has been attributed to the fact that cancer cells already have higher intracellular ROS concentrations than normal cells, and thus they have more difficulties to cope with extra oxidative damage caused by RONS from the plasma, while normal cells can defend themselves more easily, and thus reduce the oxidative stress and restore the balance²⁴. In addition, other explanations have been put forward as well, such as a higher concentration of aquaporins in the plasma membrane of cancer cells, which can transport H_2O_2 from the plasma inside the cells²⁵, and a lower concentration of cholesterol in the plasma membrane of cancer cells, which facilitates pore formation, and thus again enhances the transport of RONS from the plasma inside the cells^{26,27}.

Direct CAP treatment of cancer cells or tissue also has some drawbacks, such as the need for a standardized plasma source and the way of delivery in the body, which can make it cumbersome for treatment of some organs.

¹Research group PLASMANT, Department of Chemistry, University of Antwerp Universiteitsplein 1, BE-2610, Wilrijk-Antwerp, Belgium. ²Center for Oncological Research (CORE), University of Antwerp Universiteitsplein 1, BE-2610, Wilrijk-Antwerp, Belgium. ³Research group PPES, Department of Biomedical Sciences, University of Antwerp Universiteitsplein 1, BE-2610, Wilrijk-Antwerp, Belgium. Correspondence and requests for materials should be addressed to W.V. (email: wilma.vanboxem@uantwerpen.be) or A.B. (email: annemie.bogaerts@uantwerpen.be)

Therefore, plasma-activated cell media (PAM) or plasma-activated liquids (PAL) have gained increasing interest for cancer treatment^{18,28–37}. Until now, the focus was mainly on the use of cell media for the plasma treatment of cancer cells. For instance, Sato *et al.* showed that PAM leads to killing of HeLa cells²⁸ and Tanaka *et al.* observed that PAM selectively kills glioblastoma brain tumor cells and induces morphological changes consistent with apoptosis¹⁵. Vermeulen *et al.* compared CAP and PAM treatment for two melanoma and two glioblastoma cancer cell lines, in different plasma gas mixtures¹⁸. Recently, Canal *et al.* showed that the effect of direct treatment of cells is comparable to that of the indirect treatment of cell medium that is subsequently added to the cells²⁹. Some efforts are also undertaken to exactly control the anti-cancer activity of PAM. Yan *et al.* pointed out that the killing capability of PAM can be controlled by regulating the concentration of fetal bovine serum (FBS) in media³⁰. Furthermore, they showed that the addition of selected amino acids to the media can either enhance or reduce the anti-cancer effect of PAM^{31,32}. Adachi *et al.* demonstrated that PAM stored at $-80\text{ }^{\circ}\text{C}$ can remain stable for at least a week³³. In general, PAM seems to have similar anti-cancer effects as direct CAP treatment, but it can be more generally applied, by directly injecting it into the tissue of patients.

Furthermore, instead of PAM, it could also be interesting to treat solutions with a more simple composition with plasma, and to apply these plasma-treated solutions to cancer cells. Certainly in a clinical setting, they can be seen as more standardized solutions, and they are also more suitable for the investigation of the species and mechanisms playing an important role in the anti-cancer activity of PAL, because they are not cell line dependent. Phosphate buffered saline (PBS) is an example of a simple buffered solution. Yan *et al.*³⁴ showed that plasma-treated PBS (pPBS) is more stable than PAM, which is an advantage for the storage of this PAL. Only recently researchers started to use PBS for plasma treatment of cancer cells^{17,32,35–38}. Wende *et al.*³⁵ studied the differences between two plasma jets and the influence of ROS scavengers on the cell cytotoxicity, as well as on the concentration of H_2O_2 . Boehm *et al.*³⁶ investigated the cytotoxic and mutagenic effects of different solutions exposed to plasma, such as cell media, FBS and PBS. Yan *et al.*³² reported that the degradation of PAM, which they consider as the main disadvantage of PAM, can be stabilized by using pPBS. In a subsequent study, Yan *et al.*³⁷ compared the anti-cancer capacity of PAM and pPBS and concluded that the vulnerability of cancer cells to PAM/pPBS is cell-dependent. Girard *et al.*³⁸ studied the effect of pPBS on the viability of normal and cancer cells. Finally, Tanaka *et al.*³⁹ recently used Ringer's lactate solution as another simple solution for PAL, which was effective in killing glioblastoma cancer cells both *in vitro* and *in vivo*, due to the formation of secondary species formed via interaction of lactate with plasma RONS.

The advantages of using PAM and pPBS, or PAL in general, are rather clear, however, their anti-cancer potential is still only scarcely explored, mainly because the underlying mechanisms are largely unknown. The liquid phase chemistry of solutions exposed to plasma is quite complicated. Recently, a very comprehensive review paper was published on plasma-liquid interactions, stating the upcoming challenges, as well as the fact that there are many unresolved questions in plasma-liquid interaction⁴⁰. Measuring the RONS concentrations in PAM and PAL is gaining increasing interest in recent years^{40–44}, because they play key roles in the mechanisms taking place at cellular levels. Knowing which species are present can provide information to reveal the mechanisms taking place in the plasma treatment of cancer cells. Several RONS are suggested to play a role in the anti-cancer effect of CAP, such as OH, O_2^- , O, NO, H_2O_2 , NO_2^- , NO_3^- , ONOO, NO_2 and ONOO⁻⁴. However, when using PAL or PAM, only the long-lived species are of interest. H_2O_2 ^{31–33,45–48} and NO_2^- ^{38,49} have been regarded as the key species in the anti-cancer activity of PAM. In the context of pPBS, only few studies on the effect of RONS on the cancer cells have been published. Girard *et al.*³⁸ measured the concentrations of H_2O_2 , NO_2^- and NO_3^- in pPBS and found that H_2O_2 and NO_2^- have a synergistic effect on the anti-cancer capacity of pPBS, while NO_3^- does not contribute to the killing of cancer cells. They also investigated the effects of treatment time and gas flow rate on these concentrations, but they only considered one or two different operating conditions for plasma treatment. Yan *et al.*³⁷ showed that NO_2^- alone has no killing capacity for cancer cells, while H_2O_2 does.

In the present paper, we focus on the effect of the long-lived species NO_2^- and H_2O_2 , produced in plasma-treated PBS (pPBS). In addition to the experiments, we also perform chemical kinetics simulations to elucidate the underlying mechanisms of NO_2^- and H_2O_2 production and loss. We use an argon plasma jet kIN-Pen[®] in this study (see Materials and Methods). It must be noted that different plasma sources have different characteristics, which may result in different nature and amount of plasma-induced RONS, and ultimately in different biological effects. As mentioned before, H_2O_2 and NO_2^- are stated to play a key role in the anti-cancer effects of plasma treatment. Moreover, they can be easily identified, which is needed when considering many different conditions of plasma treatment. It is shown that different operating conditions (i.e. gap, treated volume, size of wells, etc.) have great influence on the concentrations of RONS and the anti-cancer capacity of PAM (e.g. ref.³¹) and therefore more efforts are needed to find the optimal operating conditions when treating liquids for plasma treatment. To identify the role of NO_2^- and H_2O_2 in pPBS for plasma cancer treatment, we will measure their concentrations in pPBS, for several different operating conditions. Specifically, we will determine the effect of gas flow rate, gap, treatment time and occurrence of discharges on the liquid on these concentrations, and correlate the latter with the cell cytotoxicity effect of pPBS for exactly the same conditions. While the effects of (some of) these conditions have been investigated for PAM treatment in literature, to the best of our knowledge, they have never been studied for pPBS. The composition of PBS is quite different from that of PAM, and this may lead to specific trends in the effects of the operational conditions.

To correlate the chemical composition of pPBS with its anti-cancer capacity, we consider three different cell lines of glioblastoma multiforme (GBM). GBM is the most common and lethal type of primary brain tumours⁵⁰, classified as the highest rank for tumours of the central nervous system, as issued by the WHO⁵¹. These tumours are characterised by a high invasiveness, molecular heterogeneity and rapid spreading throughout the brain⁵¹. Furthermore, they exhibit a particular resistance to surgical and medical treatment and are extremely susceptible to relapse, leading to a poor median life-expectancy of 14.6 months and a 5-year survival rate of only 9.8% when

Condition	Gas flow rate (slm)	Gap (mm)	Treatment time (min)
1	1	10	5
2	1	10	9
3	1	15	5
4	1	15	9
5	1	30	5
6	1	30	9
7	2	20	7
8	3	10	5
9	3	10	9
10	3	30	5
11	3	30	9

Table 1. List of conditions. Plasma treatment conditions applied for creating pPBS, for both the chemical analysis and the effect on the cancer cell cytotoxicity.

treated with conventional therapy⁵². These numbers indicate that the treatment remains palliative in most cases, demonstrating the need for alternative approaches, such as plasma treatment.

Materials and Methods

Plasma jet device. For the plasma treatments, we use the kINPen® IND plasma jet (INP Greifswald/neoplas tools GmbH, Greifswald, Germany). It consists of a metal cap with a pin electrode (1 mm diameter) in the middle, that is separated by a dielectric capillary (internal diameter 1.6 mm) from a grounded ring electrode^{53,54}. The plasma is created by applying a sinusoidal voltage (2–6 kV_{pp}) to the central electrode, with a frequency between 1.0 and 1.1 MHz, and a maximum power of 3.5 W. To limit the temperature, the device operates in burst mode, i.e., the plasma is switched on and off with a frequency of 2.5 kHz and a duty cycle of 50%. The plasma is created inside the capillary, after which the reactive plasma species are carried with the gas flow towards the open side of the device, creating a plasma effluent with length of 9–12 mm and diameter of 1 mm⁵³.

Cell culture. We evaluate the anti-cancer effect of pPBS for three human GBM cell lines (U87, U251 and LN229), which are grown in Dulbecco's Modified Eagle Medium (DMEM) (Gibco™ DMEM, Life Technologies, 10938025), to which we add 10% fetal bovine serum (FBS) (Gibco™ FBS, Life Technologies, 10270098), 2 mM L-glutamine (Gibco™, Life Technologies, 25030081), 100 units/mL penicilline and 100 µg/mL streptomycine (Gibco™, Life Technologies, 15140163). The cells are incubated at 37 °C and 5% CO₂.

Plasma treatment of PBS. We apply the plasma jet to treat 2 mL PBS (pH 7.3) in a 12-well plate. We use argon gas (purity 99.999%) with a flow rate of 1–3 slm. We study the effect of three important plasma treatment parameters, i.e., gas flow rate, gap between device outlet and treated solution, and treatment time, as well as the effect of the occurrence of discharges at the liquid surface. The conditions used to link the chemical composition of pPBS with the cancer cell cytotoxicity (see below) are listed in Table 1.

For conditions 1 and 2 the gap is small enough to have discharges at the liquid surface, more specifically, discharge streamers are visible between the head of the plasma jet and the liquid surface. In this case, the liquid surface acts as a third electrode, and the electrons start playing a role inside the liquid, by causing electron impact reactions. Note that when the gap is only 10 mm, but a higher flow rate of 3 slm is applied (conditions 8 and 9), no discharges take place, because the liquid is blown towards the sides of the well. For conditions 3 and 4 the gap is just large enough (i.e. 15 mm instead of 10 mm) to avoid the discharges.

Besides the conditions of Table 1, we also perform a more detailed study on the effect of plasma treatment time on the concentrations of NO₂⁻ and H₂O₂ in pPBS and on the cancer cell cytotoxicity. For this purpose, we apply a gas flow rate of 1 slm, 10 mm gap (i.e., condition 1 of Table 1), and plasma treatment times of 5 min, 2 min 30 sec, 1 min 15 sec, 37.5 sec and 18.75 sec. These treatment times are obtained by so-called “diluting” the treatment time consecutively by a factor of two.

Quantification of H₂O₂ in pPBS. For the detection of H₂O₂ we apply colourimetry, using the titanium sulphate method⁵⁵. In acid environment, H₂O₂ reacts with Ti⁴⁺ ions, forming a yellow peroxytitanium(IV) complex (reaction R.1), which has an absorption maximum around 407 nm. This complex is stable for at least 6 hours⁵⁶. After plasma treatment, NaN₃ is added to this solution to avoid the destruction of H₂O₂ by NO₂⁻ (reaction R.2)⁵⁷. Indeed, NaN₃ reacts with NO₂⁻ according to reaction R.3, so that NO₂⁻ disappears from the solution⁵⁸. As these reactions occur in acidic environment, it is important to add the azide before the acid titanium(IV)-solution⁵⁶.





The analysis is performed with a ThermoFischer Genesys™ 6 spectrophotometer. The cuvettes are made of quartz, and have a path length of 1 cm, a volume of 700 μL and an internal width of 2 mm. We measure the absorbance comparing with a blank solution at 400 nm. For this purpose, we prepare a solution of 80 mM NaN_3 in PBS and a solution of 0.1 M $\text{K}_2\text{TiO}(\text{C}_2\text{O}_4)_2 \cdot 2\text{H}_2\text{O}$ (Sigma Aldrich®, 14007) and 5 M H_2SO_4 in milli-Q water. For the measurements, we add 50 μL N_3^- solution, 200 μL pPBS and 50 μL Ti(IV)-solution to the cuvette. Concentrations are calculated based on the extinction coefficient determined in a calibration experiment (Supplementary Figure S1).

Quantification of NO_2^- in pPBS. For measuring the NO_2^- concentration, we use the Griess method⁵⁹ (Griess Reagent Nitrite Measurement kit, Cell Signaling Technology®, 13547).

The analysis occurs in a 96-well plate with a BIO-RAD iMark™ Microplate reader. 100 μL Griess reagent (1:1 sulfanilamide and *N*-(1-naftyl)-ethylenediamine) and 100 μL pPBS are added to each well. Also a blank solution is made in the well plate. The absorbance is measured in triplicate. Concentrations are calculated based on the extinction coefficient determined in a calibration experiment (Supplementary Figure S2).

Measurement of O_3 in pPBS. We also tried to detect O_3 in the pPBS by means of electron paramagnetic resonance spectroscopy (EPR). The analysis occurs in Ringcaps® 50 μL capillaries with a MiniScope MS 200 (Magnettech) spectrometer. The measurements are performed by adding 4-oxo-TEMP (2,2,6,6-tetramethyl-4-piperidone) to pPBS. 4-oxo-TEMP was reported to react with ozone to produce a stable nitroxide radical 4-oxo-TEMPO (4-oxo-2,2,6,6-tetramethyl-4-piperidinyloxy).⁴³ In our case, no radical formation is detected.

Treatment of cancer cells with pPBS. Before the treatment with pPBS, the U87 and LN229 cells are plated at 3000 cells per well, while the U251 cells are plated at 1500 cells per well in 150 μL medium in a 96-well plate. These seeding densities are based on our previous experience, as they appear to be suitable for our purposes. After incubation for 24 hours at 37 °C and 5% CO_2 , the cells are treated with pPBS. For this purpose, we apply 30 μL of the pPBS to the 150 μL cells and medium present in the wells (which corresponds to a ratio of 1/6).

We also perform experiments in which catalase is added to the pPBS, as a scavenger for H_2O_2 , in order to verify the role of H_2O_2 in the cancer cell cytotoxicity. For this purpose, 400 U mL^{-1} of catalase is added to the pPBS, after which the solution is stirred for 10–15 minutes. After this, 30 μL of pPBS + catalase is added to the cells in 150 μL medium. This experiment is carried out for conditions 1, 4, 6, 8, and 10.

Treatment of cancer cells with H_2O_2 and/or NO_2^- rich PBS. We also want to verify whether only the H_2O_2 or NO_2^- in the pPBS is responsible for the anti-cancer capacity, or whether it is the cocktail of species that is important. For this purpose, we compare the anti-cancer capacity of pPBS with that of PBS to which H_2O_2 and/or NO_2^- (as NaNO_2) is added. Different solutions of PBS containing H_2O_2 , NO_2^- , or a mixture of both are prepared. The concentrations of H_2O_2 and NO_2^- are the same as in the pPBS for the conditions considered, i.e. conditions 1, 4, 6, 8, and 10. To treat the cells, 30 μL of the H_2O_2 and/or NO_2^- rich PBS solution is added to the cells in 150 μL medium.

Stability of pPBS. We also investigate the stability of pPBS by applying a gas flow rate of 1 slm, a gap of 15 mm and a treatment time of 5 min (i.e., condition 3 of Table 1). In a first set of experiments, we analyse the pPBS, and we add it to the cells, at fixed time steps after treatment, i.e., after 0 min, 5 min, 10 min, 30 min, 60 min and 120 min. In a second set of experiments, we assess the stability of cell medium to which we add pPBS (in a ratio of 1/6), by again analysing the chemical composition in this medium and by adding 180 μL of this medium to the cells (after removal of their original medium) at the same fixed time steps after treatment. For the chemical composition, we could only analyse the concentration of NO_2^- , because in the case of H_2O_2 , the air bubbles present in the cell medium after shaking the cuvette make it impossible to measure the solution in the spectrometer.

Cell cytotoxicity assay. After the treatment with pPBS, we analyse the cell cytotoxicity (meaning both cytostatic and cytotoxic effects) by the sulforhodamine B-method (SRB)⁶⁰. After removing the medium, the cells are fixed with 10% trichloroacetic acid (TCA). After washing away the TCA and the dead cells that are still present, we add 100 μL SRB (Sigma-Aldrich®, S1402) to each well. After thorough washing of the non-bound dye with 1% (vol/vol) acetic acid, and dissolving the bound dye with 100 μL tris-buffer (tris(hydroxymethyl)aminomethane, Sigma-Aldrich®, 252859), we measure the absorbance with the BIO-RAD iMark Microplate reader. The cell cytotoxicity is determined by comparing with an untreated control sample.

Description of the model. To elucidate the underlying mechanisms responsible for the production and loss of H_2O_2 and NO_2^- in the pPBS, we also performed computer simulations with a 0D chemical kinetics model for the plasma jet in contact with liquid water. This model is based on solving balance equations for the different species, based on production and loss terms. In total, 91 different species and 1390 different chemical reactions are included in the gas phase (plasma jet in contact with ambient air) and 35 different species and 89 different chemical reactions are considered in the liquid phase. More details about the model, and the assumptions made to mimic the experimental conditions, are given in the Supplementary Information.

Data availability statement. All data generated or analysed during this study are included in this published article (and its Supplementary Information).

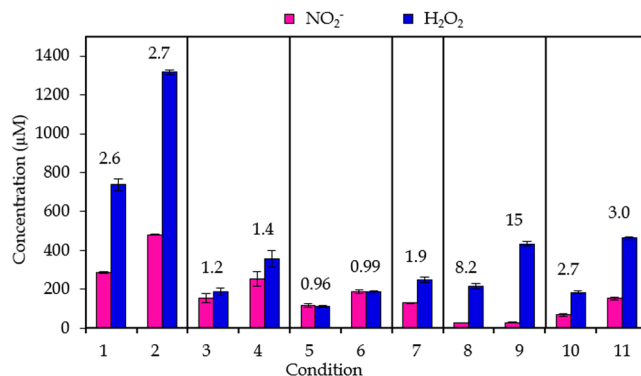


Figure 1. Results for chemical composition. Concentrations of NO₂⁻ and H₂O₂ in pPBS at the 11 plasma treatment conditions listed in Table 1. Conditions for which only the plasma treatment time differs are indicated within one frame. The concentrations are plotted as the mean of at least three repetitions, and the error bars indicate the standard deviations of the mean. The numbers above the signals indicate the ratio of the concentration of H₂O₂ to the concentration of NO₂⁻ for that condition.

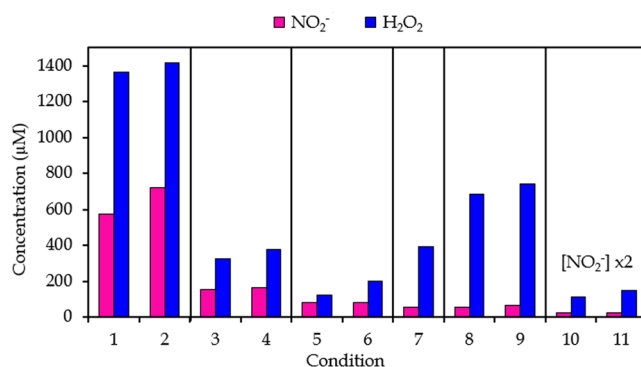


Figure 2. Overview of the computational results. Concentrations of NO₂⁻ and H₂O₂ at the 11 plasma treatment conditions listed in Table 1, as obtained from the chemical kinetics model (see SI). Conditions for which only the plasma treatment time differs are indicated within one frame.

Results and Discussion

H₂O₂ and NO₂⁻ are present at different ratios in pPBS when applying different operational conditions, but in all cases H₂O₂ has a higher concentration. Figure 1 presents the measured concentrations of NO₂⁻ and H₂O₂ at the 11 conditions listed in Table 1 above. The ratios of the concentrations of NO₂⁻ and H₂O₂ are also indicated in the figure. It is clear that the concentration of H₂O₂ is always larger than that of NO₂⁻. Comparing conditions where the gas flow rate and gap are kept constant but only the plasma treatment time is varied, tells us that the ratio of the concentrations is kept the same, except for conditions 8 and 9, where the concentration of NO₂⁻ is extremely low. Thus, a high gas flow rate and small gap (conditions 8 and 9) favor the formation of H₂O₂ compared to NO₂⁻. Vice versa, at a low gas flow rate and a large gap (conditions 5 and 6), the concentrations of NO₂⁻ and H₂O₂ are comparable, indicating that the formation of NO₂⁻ is promoted.

The fact that different concentrations of species are formed by varying the plasma treatment conditions might be important in terms of the application, as some species will be more effective in killing the cancer cells, or might act even more selectively towards cancer cells than normal cells, in comparison to other species. Thus, by varying the plasma treatment parameters, the concentration of these particular species can be promoted.

Chemical kinetics modelling elucidates the most important source and loss processes for the generation of H₂O₂ and NO₂⁻.

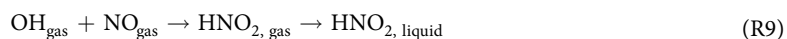
Figure 2 presents the calculated liquid-phase concentrations of NO₂⁻ and H₂O₂ as obtained from the model described in the Supplementary Information, at the 11 conditions listed in Table 1. When comparing these results to the experimental data of Fig. 1, a reasonable agreement is observed. Indeed, although an exact quantitative agreement cannot be expected, due to the many assumptions made when using a chemical kinetics model, similar trends are observed in both the calculations and the experiments, in terms of (i) absolute values, (ii) higher H₂O₂ vs NO₂⁻ concentrations at (nearly) all conditions, and (iii) variations in concentrations as a function of plasma treatment time, gas flow rate, gap, and the presence of discharges onto the liquid surface. This indicates that the chemical kinetics model provides a realistic picture of the gas-phase and liquid-phase chemistry over the entire range of conditions investigated, and can thus be used to elucidate the underlying mechanisms at these various conditions. A general scheme which includes the main pathways leading to the generation and loss of H₂O₂ and NO₂⁻, as predicted by the model, is depicted in Fig. 3.

Condition	Contribution R.9 (%)	Contribution R.10 (%)	Contribution R.11 (%)
1-2	67	26	7
3-4	67	25	8
5-6	68	5	27
7	63	31	6
8-9	27	68	5
10-11	53	43	4

Table 3. NO_2^- generation. Contribution of different pathways to the generation of aqueous NO_2^- .

gas density is much higher than that of O-species (~80% of ambient air consists of N_2). This has a double effect on the aqueous H_2O_2 concentration: (i) the gaseous density of H_2O_2 will not increase upon increasing gap, so its contribution to the aqueous H_2O_2 is very similar in all cases (at the same flow rate), but (ii) because the aqueous OH concentration is significantly lower at larger gap, the recombination rate into H_2O_2 in the liquid phase will be much lower. Consequently, the aqueous H_2O_2 concentration will decrease upon increasing gap.

For NO_2^- , a similar analysis can be done. NO_2^- in the liquid is in balance with HNO_2 (see Fig. 3). The latter is mainly generated in the liquid by three processes:



The relative contribution again depends on the treatment conditions and is shown in Table 3.

At 1 slm flow rate, ambient air species can easily diffuse into the plasma effluent, and thus the HNO_2 concentration will already become very large in the gas phase, which explains why it is the most important source of aqueous HNO_2 . Upon increasing flow rate, it will become more difficult for ambient air species to diffuse into the plasma effluent. Moreover, the species that are initially generated in the gas phase (i.e. OH and NO) have less time to recombine before reaching the liquid phase. Hence, the relative contribution of R.9 decreases (most prominent when compared at 10 mm gap). By increasing the gap, the species have again more time to recombine in the gas phase, and thus the contribution of R.9 will increase again compared to R.10 (most prominent when compared at 3 slm).

In order to explain the absolute concentrations of NO_2^- for the different conditions investigated, we have to keep in mind that to generate any of the HNO_2 (and thus NO_2^-) generating species (cf. R.9–11), both O_2 and N_2 are required. As mentioned before, by increasing the flow rate, the ability of these ambient air species to diffuse into the plasma effluent will drop. Therefore, the HNO_2 concentration measured in the liquid is much more dependent on the gas flow rate than H_2O_2 , as can be derived from Figs 1 and 2.

Moreover, Fig. 3 illustrates that the main loss process of NO_2^- is the reaction with O_3 :



By increasing the gap, the amount of O_2 that can diffuse into the plasma effluent will rise, and thus also the amount of O_3 generated in the plasma effluent. This gaseous O_3 is subsequently transported into the liquid, where it will react with NO_2^- . This explains the drop in NO_2^- concentration upon increasing gap (see Figs 1 and 2).

In summary, our model predicts that both H_2O_2 and NO_2^- can be generated either (i) from diffusion of these species from the gas phase, or (ii) from aqueous reactions of short-lived species, and the relative contribution of both pathways strongly depends on the treatment conditions (flow rate and gap).

H_2O_2 , rather than NO_2^- , is the more important species for cancer cell cytotoxicity. Figure 4 presents the percentages of cell cytotoxicity for the three cell lines, along with the concentrations of NO_2^- and H_2O_2 shown in Fig. 1, at exactly the same conditions to make the correlation between both. To evaluate whether pPBS has the same effect on cell cytotoxicity for all three cell lines, we carried out a non-parametric t-test, which indicated that for the 99% confidentiality interval only condition 11 yielded a significant difference between the cell cytotoxicity for cell lines U251 and LN229 on one hand, and for U87 on the other hand. At all other conditions, the cell cytotoxicity could be considered similar for the three cell lines. There are some differences, but they can be attributed to different air humidity during the experiments, and to a different cell growth rate for the different cell lines. Indeed, when the cell lines exhibit different growth rates after treatment, this can yield a wrong picture about their sensitivity upon treatment with pPBS, as the cell survival was evaluated by the SRB method, where the total amount of proteins is a measure for the viability with respect to an untreated control sample. However, in this study we focus on the correlation between cell cytotoxicity and NO_2^- and H_2O_2 concentrations in pPBS for different plasma treatment conditions. Therefore, we will not further elaborate on the different sensitivity for the different cell lines.

In order to compare the concentrations of NO_2^- and H_2O_2 with the percentage of cell cytotoxicity for all conditions investigated, it is important to note that the results of the latter are always limited to a maximum of

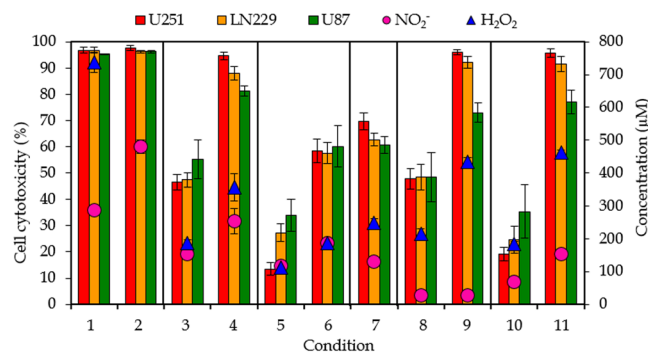


Figure 4. General overview of the results. Effect of pPBS on cancer cell cytotoxicity for three different GBM cell lines (U251, LN229 and U87) (left y-axis), and comparison with the concentrations of NO_2^- and H_2O_2 in pPBS (right y-axis), for the 11 conditions listed in Table 1. Note that the H_2O_2 concentration in condition 2 is 1317 μM , but this is deliberately out of scale, to better evaluate the correlation between cell cytotoxicity and chemical composition for all other conditions. Conditions that only differ in plasma treatment time are indicated within one frame. The concentrations and percentages are plotted as the mean of at least three repetitions, and the error bars indicate the standard deviations of the mean.

100% cell cytotoxicity, while the concentrations of NO_2^- and H_2O_2 are not limited and can be higher than the concentrations needed to achieve 100% cell cytotoxicity. As a first tool for the determination of the most important species for the anti-cancer capacity of pPBS, we compare the trends between the cell cytotoxicity and the concentrations of the reactive species over all the operating conditions applied.

It is evident from Fig. 4 that the percentages of cell cytotoxicity exhibit the same trends as the concentrations of H_2O_2 , but do not correlate with the concentrations of NO_2^- . Indeed, when the concentration of H_2O_2 raises, a higher percentage of cell cytotoxicity is obtained, and vice-versa. On the other hand, at conditions 8 and 9, there is almost no NO_2^- present in pPBS, while we observe a high percentage of cell cytotoxicity. Likewise, at conditions 3 and 11, the concentration of NO_2^- in pPBS is very similar, while condition 11 causes twice as much cell cytotoxicity as condition 3. Thus, we may conclude from this overview that H_2O_2 most probably plays a more important role in cancer cell cytotoxicity than NO_2^- , because the cell cytotoxicity follows the same trends as the H_2O_2 concentration over all the operating conditions. However, other species, like NO , NO_3^- and ONOOH , can be important as well, either for killing the cancer cells, or for promoting the selectivity between cancer and normal cells (for which NO_2^- may also play a role).

To further prove this statement, we perform experiments in which we add catalase to the pPBS after plasma treatment. Catalase is a scavenger for H_2O_2 and by adding it to the pPBS after plasma treatment, the H_2O_2 will be removed from the solution. For the conditions investigated (conditions 1, 4, 6, 8, and 10), adding the catalase results in no observed cell cytotoxicity in all cases (Supplementary Figure S5). This means that H_2O_2 indeed plays an important role for the anti-cancer activity of pPBS. From these experiments, one would expect H_2O_2 to be the only important species. However, further results demonstrate that this is not the case, and other plasma-induced RONS must be present in the system.

Sato *et al.*²⁸ also showed that indeed H_2O_2 is most probably the dominant RONS inducing cancer cell death when using PAM.

H_2O_2 and/or NO_2^- rich PBS has not the same effect on cancer cells as pPBS. Figure 5 presents the results of the experiments where we used H_2O_2 and/or NO_2^- rich PBS to compare the effect on cell cytotoxicity with pPBS. The concentrations of the reactive species added to PBS match these in the pPBS for the conditions considered. Firstly, it is clear that NO_2^- alone has no killing effect on GBM cancer cells in any case. On the other hand, the H_2O_2 rich PBS is able to kill the cancer cells in all conditions for the U87 cell line. For U251 cells, the H_2O_2 rich PBS has only a killing effect for conditions 1 and 4, and for the LN229 cells H_2O_2 significantly kills cancer cells in all conditions, except 8. This reveals that H_2O_2 indeed contributes to the cancer cell cytotoxicity in most cases, but it cannot be the only important species. When we consider both H_2O_2 and NO_2^- in PBS, there is mostly no additional killing effect observed, except for the U87 cell line, where in all cases a synergistic effect of H_2O_2 and NO_2^- is observed. We can conclude that the cell lines react differently on the addition of these reactive species, while the overall effect of pPBS on the three cell lines seems comparable (see above).

This also suggests that catalase, as a scavenger of H_2O_2 , does not only scavenge H_2O_2 , but also other reactive species that appear to be important for the anti-cancer activity of pPBS. Indeed, catalase possibly scavenges peroxynitrite (ONOO^-) too⁶¹, and possibly other RONS.

Girard *et al.*³⁸ reported a synergistic effect of H_2O_2 and NO_2^- when using pPBS on colon cancer and melanoma cells, which is in correlation with our results for the U87 cell line. Yan *et al.*³¹ demonstrated that adding only H_2O_2 to cancer cells does not have the same effect as PAM treatment, suggesting that other RONS also play a role. Kurake *et al.*⁴⁹ reported that other RONS than H_2O_2 and NO_2^- also participate in the anti-cancer capacity when using PAM, and found a synergistic effect of H_2O_2 and NO_2^- on U251 cells. However, they used another plasma source that produces significantly higher relative amounts of NO_2^- compared to the plasma jet used in our study. Indeed, while we always have higher amounts of H_2O_2 present in the pPBS, they measure NO_2^- concentrations that are 30 times greater than that of H_2O_2 .

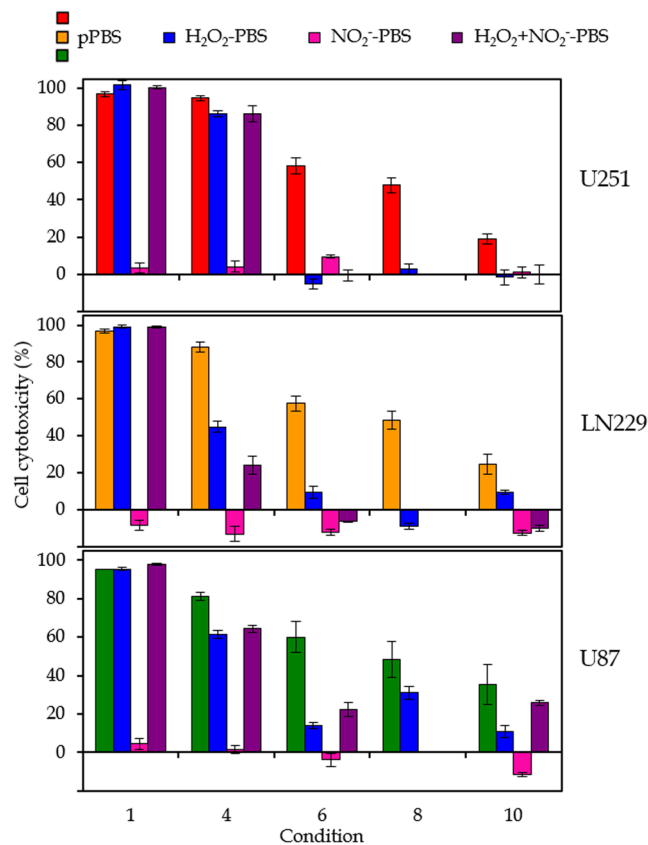


Figure 5. Effect of H_2O_2 and/or NO_2^- rich PBS on cell cytotoxicity. Comparison of the effect of pPBS with H_2O_2 and/or NO_2^- rich PBS on the cell cytotoxicity for three different GBM cell lines (U251, LN229 and U87). The concentrations of H_2O_2 and/or NO_2^- match these in the pPBS for the conditions considered (i.e. conditions 1, 4, 6, 8 and 10, which are listed in Table 1). For condition 8, no significant amount of NO_2^- is measured in the pPBS. Hence, only H_2O_2 rich medium is tested for that condition. The percentages are plotted as the mean of at least three repetitions, and the error bars indicate the standard deviations of the mean.

Condition	Gas flow rate (slm)	Gap (mm)	NO_2^-	H_2O_2	U251	LN229	U87
1-2	1	10	1.67 ± 0.03	1.79 ± 0.08	/	/	/
3-4	1	15	1.6 ± 0.3	1.9 ± 0.3	2.0 ± 0.1	1.9 ± 0.1	1.5 ± 0.2
5-6	1	30	1.6 ± 0.2	1.6 ± 0.1	$4.3 \pm 0.8^*$	2.1 ± 0.3	1.8 ± 0.4
8-9	3	10	$1.1 \pm 0.1^*$	2.0 ± 0.1	2.0 ± 0.2	1.9 ± 0.2	1.5 ± 0.3
10-11	3	30	$2.3 \pm 0.2^*$	$2.5 \pm 0.1^*$	$5.0 \pm 0.7^*$	$3.7 \pm 0.8^*$	$2.2 \pm 0.6^*$

Table 4. Effect of plasma treatment time. Ratios of the concentrations of NO_2^- and H_2O_2 in pPBS and of the cell cytotoxicity for the three cell lines, for the plasma treatment times of 9 and 5 minutes, for the different conditions listed in Table 1. A ratio of 1.8 suggests a linear increase of the concentrations with treatment time. Results that significantly deviate from the linear increase are indicated with an asteriks. The values are given as the ratios of mean values of at least three repetitions \pm the standard deviation.

Overall, it is unambiguous that H_2O_2 plays one of the major roles in the anti-cancer effect of pPBS, whereas NO_2^- is less important. However, the cell cytotoxicity of pPBS cannot be explained by H_2O_2 rich PBS alone, and other reactive species must contribute to the cell cytotoxicity as well, when using pPBS.

Do the concentrations of H_2O_2 and NO_2^- , as well as the cell cytotoxicity increase linearly with plasma treatment time? From Figs 1 and 4 we can easily deduce the effect of the plasma treatment time on the concentrations of NO_2^- and H_2O_2 in the liquid and on the cell cytotoxicity, because the conditions that only differ in treatment time are plotted within one frame. The ratios of the concentrations and cell cytotoxicity, for a plasma treatment time of 9 and 5 min, are listed in Table 4 for the different conditions investigated. For the results of chemical composition, it is clear that this ratio is close to 1.8 (i.e., the ratio of the treatment times) for most conditions, except for conditions 10 and 11 (for both NO_2^- and H_2O_2) and for conditions 8 and 9 (only for NO_2^-). However, for these last conditions, the concentrations of NO_2^- are very low, making the results less

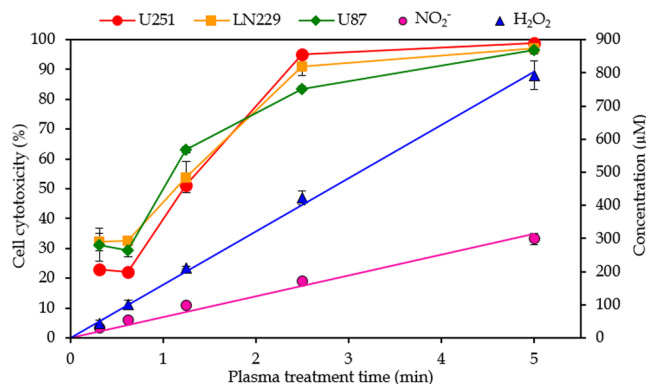


Figure 6. Effect of plasma treatment time. Concentrations of NO_2^- and H_2O_2 in pPBS (right y-axis) and cell cytotoxicity (left y-axis) as a function of plasma treatment time, for a gap of 10 mm and a gas flow rate of 1 slm (i.e., condition 1 of Table 1). The concentrations and percentages are plotted as the mean of at least three repetitions, and the error bars indicate the standard deviations of the mean.

reliable. It is yet unclear why the ratio at conditions 10 and 11 (i.e., high flow rate and large gap) is different from 1.8.

For the effect of the plasma treatment time on the cancer cell survival, we cannot use the results of conditions 1 and 2, because they both reach 100% cell cytotoxicity (cf. Figure 4). It is clear from Table 4 that the ratios of the percentage cell cytotoxicity are again close to 1.8, except for conditions 10 and 11 (which is in agreement with the chemical composition), and for U251 for conditions 5 and 6, which may be due to experimental variations.

A more detailed study of the effect of plasma treatment time was performed as well, and the results are plotted in Fig. 6. The concentrations of NO_2^- and H_2O_2 indeed rise linearly with increasing plasma treatment time, until a time of about 5 minutes, at the conditions of gap and gas flow rate investigated here (i.e., 10 mm and 1 slm). We did not apply longer treatment times here, but Table 4 indeed suggests that this linearity more or less continues up to 9 minutes. Yan *et al.*³¹ also demonstrated a linear rise in the concentrations of RNS and H_2O_2 in PAM for a treatment time up to 2 minutes, when using a helium plasma jet. We may conclude from our results that up to 9 minutes of plasma treatment no saturation of the plasma species in the pPBS occurs.

For the effect on the cell cytotoxicity, the shortest plasma treatment time (18.75 sec) apparently yields more or less the same cell cytotoxicity as the treatment time of 37.5 sec. Hence, it seems that small amounts of plasma species in the pPBS already give some cell cytotoxicity but that the effect is not linear here. On the other hand, a treatment time of 5 minutes results in 100% cell cytotoxicity at these conditions, so this data point cannot be considered for evaluating the linearity, as 100% cell cytotoxicity will be reached already somewhere between 2.5 and 5 min. It seems that the cell cytotoxicity does not increase linearly with treatment time for the U87 cell line, while the U251 and LN229 cell lines exhibit a more linear behaviour, although this is again based on only three data points. Several studies also reported a more or less linear effect of the plasma treatment time on cell death¹⁹ or RONS concentrations^{14,38,49} when using PAM, albeit also with some deviations.

Increasing the gap results in lower concentrations of NO_2^- and H_2O_2 and less cell cytotoxicity.

The effect of the gap on the chemical composition of pPBS and the cell cytotoxicity is illustrated in Fig. 7(a,b,e,f). At a gas flow rate of 1 slm (Fig. 7(a)), both the concentrations of NO_2^- and H_2O_2 show a drop upon increasing gap from 15 to 30 mm, although the drop is more pronounced for H_2O_2 than for NO_2^- . Yan *et al.*³¹ and Takeda *et al.*⁶² also reported such a drop upon increasing gap when using PAM. This drop can be explained because the reactive plasma species are present in the gas phase for a longer time, so they have more chance to get lost upon reaction with other species. Hence, a lower amount of reactive plasma species (i.e. OH radicals for the H_2O_2 generation, and OH and NO radicals for the NO_2^- generation, cf. modelling results above) arrive in the liquid, explaining the lower concentrations of NO_2^- and H_2O_2 . For NO_2^- an additional explanation is provided by the modelling results above. A higher gap results in the formation of more O_3 , which will react with NO_2^- in the liquid, lowering its concentration. On the other hand, at a gas flow rate of 3 slm (Fig. 7(b)), the NO_2^- concentration rises upon increasing gap. It seems that this flow rate is high enough to transport the RONS into the liquid, without the risk for them to get lost by reactions. However, as the concentration of NO_2^- at conditions 8 and 9 is extremely low, we cannot draw conclusions from this trend. For H_2O_2 the effect of the gap looks negligible at a gas flow rate of 3 slm. As mentioned above, we expect the concentration of H_2O_2 to be dependent on the reactions of OH radicals, either in the gas or in the liquid phase. At a gas flow rate of 3 slm, increasing the gap will have no significant effect on the H_2O_2 concentration, because the gas flow rate is high enough to enable the remaining OH radicals (not yet recombined to H_2O_2 in the gas phase) to reach the liquid, independent from the gap.

Figure 7(e,f) also demonstrates that a larger gap results in less cell cytotoxicity, both at 1 and 3 slm. Only for a treatment time of 9 min with a gas flow rate of 3 slm, the gap seems to have no effect. This might be correlated to the fact that the concentration of H_2O_2 at these conditions is also the same, thus pointing towards the important role of H_2O_2 in causing cell cytotoxicity. In general, the effect of the gap seems to be the same on the cell

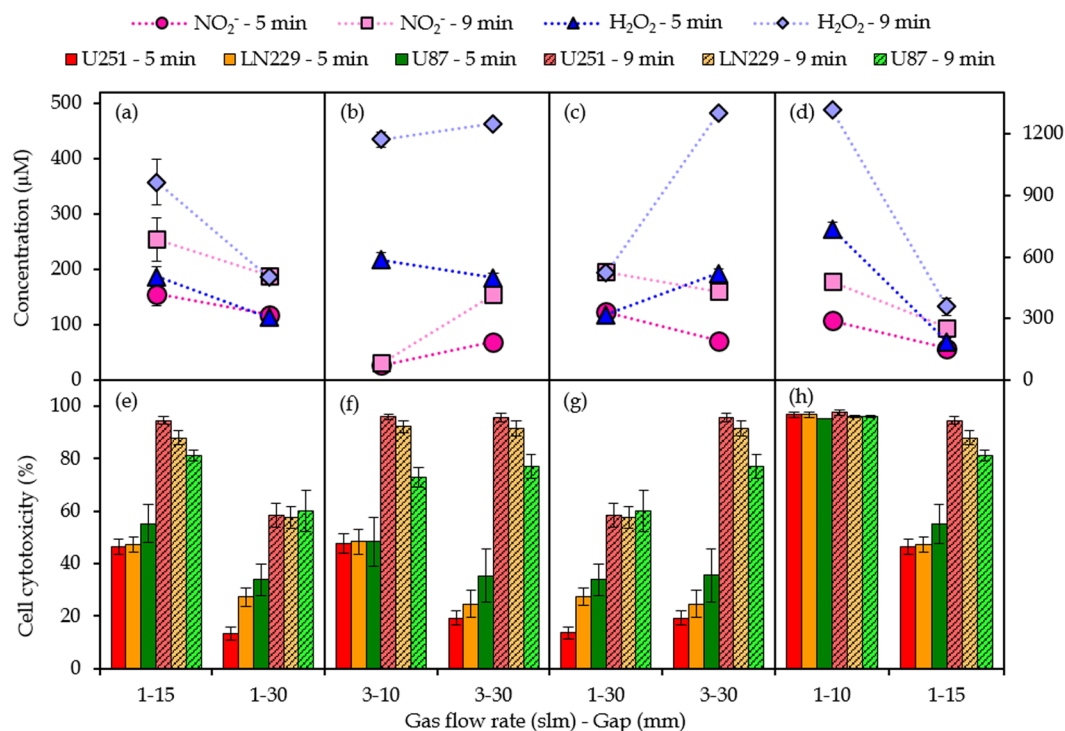


Figure 7. Effect of plasma treatment parameters. Effect of the gap (a,b,e,f), gas flow rate (c,g) and discharges at the liquid surface (d,h) on the concentrations of NO_2^- and H_2O_2 in pPBS (a–d) and on the cell cytotoxicity for the three cell lines (e–f). For the effect of the discharges, the concentrations of NO_2^- and H_2O_2 are plotted on the right y-axis. The concentrations and percentages are plotted as the mean of at least three repetitions, and the error bars indicate the standard deviations of the mean.

cytotoxicity and on the chemical composition, for both NO_2^- and H_2O_2 , but is more pronounced at lower flow rates than at higher flow rates.

The gas flow rate has an opposite effect on NO_2^- and H_2O_2 , while the cell cytotoxicity acts similarly as H_2O_2 . Figure 7(c,g) depicts the effect of the gas flow rate on the chemical composition, as well as on the cell cytotoxicity. A higher gas flow rate yields a slight drop in NO_2^- concentration, but a rise in H_2O_2 concentration. Since the concentration of NO_2^- depends on the surrounding air molecules (see above), we can state that a higher gas flow rate limits the number of air molecules that can come in contact with the plasma effluent, leading to a lower NO_2^- concentration in the liquid. On the other hand, our modelling results reveal that the H_2O_2 formation depends on (i) the H_2O_2 from the gas phase reaching the liquid phase, and (ii) the recombination of two OH radicals in the liquid. As mentioned before, at high flow rates, the fraction of gaseous OH radicals that reach the liquid is large. Since the generation of H_2O_2 molecules is linearly dependent on the OH concentration squared, a significantly higher amount of H_2O_2 will be detected. It is clear that the H_2O_2 concentration is more affected by the gas flow rate than by the gap, while both effects are comparable for the NO_2^- concentration.

A higher gas flow rate results in more cell cytotoxicity for all three cell lines. This correlates well with the trend of the H_2O_2 concentration, again suggesting that the cell cytotoxicity is primarily caused by H_2O_2 and less (or not) by NO_2^- .

Girard *et al.*³⁸ reported lower concentrations of both H_2O_2 and NO_2^- when increasing the gas flow rate. However, they applied only two conditions to conclude this, and the gas flow rate was 8 times higher in the second condition. The fact that we consider lower variations in gas flow rate can explain these different findings, demonstrating again the importance of the operating conditions during the plasma treatment.

The occurrence of discharges on the liquid has a great effect on the concentrations of reactive species and on the cell cytotoxicity. Finally, the effect of discharges at the liquid surface is presented in Fig. 7(d,h). Enlarging the gap till a distance where no discharges take place anymore at the liquid surface (i.e., 15 mm instead of 10 mm) has a striking effect on the concentrations in the liquid phase. Note that the difference shown in this figure is the combination of two effects, i.e., a large gap and the disappearance of discharges. However, it was clear from Fig. 7(a,b,e,f) that enlarging the gap in the absence of discharges at the surface only has a minor effect. Therefore, we can conclude that the effect shown in Fig. 7(d,h) is predominantly due to the presence of surface discharges. The NO_2^- concentration drops with a factor 2, while the H_2O_2 concentration even drops with a factor 4 upon disappearance of these discharges. For H_2O_2 , the occurrence of discharges onto the liquid surface results in the formation of more OH radicals in the liquid (see Table 2), due to electron impact reactions with the water molecules in PBS. As predicted by our model, this results in higher H_2O_2 concentrations (see

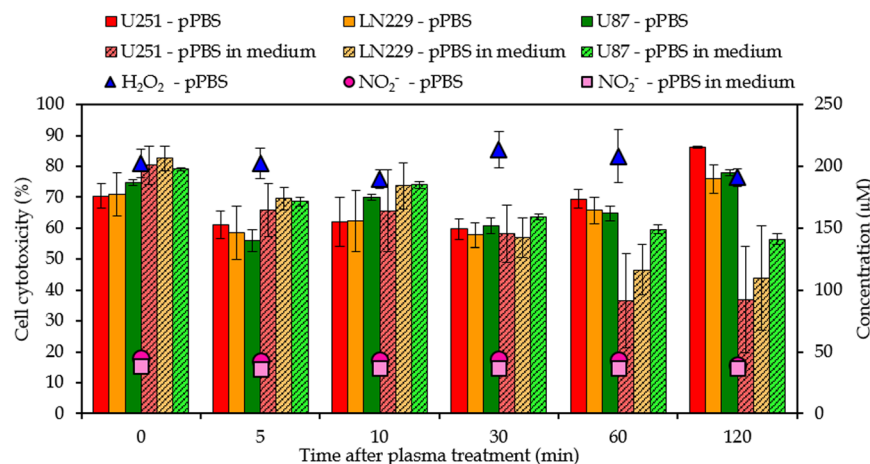


Figure 8. Stability of pPBS and pPBS with medium. Concentrations of NO_2^- and H_2O_2 (right y-axis) and cell cytotoxicity of the three cell lines (left y-axis) as a function of time after treatment, to evaluate the stability of pPBS and of pPBS with medium, for a gap of 15 mm and a gas flow rate of 1 slm (i.e., condition 3 of Table 1). The concentrations and percentages are plotted as the mean of at least three repetitions, and the error bars indicate the standard deviations of the mean.

above). On the other hand, the relative contributions for the formation of NO_2^- do not change with or without the presence of discharges (see Table 3). The electron impact reactions with the liquid have an overall rising effect on the reactive species present in both gas and liquid phase, resulting in higher NO_2^- concentrations. As the raise of H_2O_2 is higher than that of NO_2^- , we can conclude that the generation of H_2O_2 depends more on the generation of reactive species out of electron impact reactions.

As expected, the occurrence of discharges at the liquid surface results in more cell cytotoxicity. Indeed, a gap of 10 mm and flow rate of 1 slm results in 100% cell cytotoxicity, while the same flow rate but a gap of 15 mm results in ca. 50% and 90% cell cytotoxicity for a plasma treatment time of 5 and 9 min, respectively. This indicates that the occurrence of discharges at the liquid surface yields at least twice as much cell cytotoxicity, which is in agreement with the results for the chemical composition of pPBS.

PBS might be a better storage solution for RONS than cell media. As mentioned in the Introduction, it is reported in literature that PAM can be stored during 7 days at a temperature of -80°C ³³. Here we investigate the stability of pPBS at room temperature for a period of 2 hours. This would be convenient for practical applications of pPBS in a clinical setting. For this purpose, we measured the concentrations of NO_2^- and H_2O_2 in pPBS at fixed times after plasma treatment (see Fig. 8). The concentrations of NO_2^- and H_2O_2 in pPBS obviously remain constant during at least 2 hours. We also added the pPBS to the cancer cells at these times after treatment and see that the effect on the cell cytotoxicity remains constant as well (see Fig. 8).

In addition, the concentration of NO_2^- was also determined when pPBS was added to the cell medium immediately after treatment, showing again a stable concentration for at least 2 hours (see Fig. 8). Unfortunately, we could not determine the concentration of H_2O_2 in this case, as mentioned above. However, when pPBS is added to cell medium directly after treatment, the percentage cell cytotoxicity is lower when pPBS + medium is applied to the cancer cells after 30–60 min. This suggests that the reactive species in pPBS responsible for cell death react with organic molecules in the medium, so that pPBS loses part of its anti-cancer capacity when it is added to cell medium. As the concentration of NO_2^- in pPBS + medium remains constant, the reduced cell cytotoxicity will be attributed to other reactive species, possibly H_2O_2 , as it was reported that the H_2O_2 concentration in PAM drops when kept at room temperature^{33,63}. Indeed, Yan *et al.*³⁴ investigated the instability of PAM and found that H_2O_2 reacts with cysteine and methionine resulting in a lower anti-cancer capacity of the cell media. As mentioned above, we could not measure the H_2O_2 concentration in medium + pPBS, so we cannot conclude whether a drop in H_2O_2 concentration is causing this reduced cell cytotoxicity. As the concentration of H_2O_2 in pPBS (without medium) remains stable at room temperature for at least 2 hours (see Fig. 8), we tentatively conclude that PBS is a better way of storage for plasma species than cell medium itself, and thus, that pPBS could be more suitable for practical applications in a clinical setting than PAM.

Conclusion

We measured the chemical composition, more specifically the concentrations of NO_2^- and H_2O_2 , of plasma-treated PBS (pPBS) with the kINPen[®]IND plasma jet, for different values of gas flow rate, gap and plasma treatment time, and we also evaluated the effect of this pPBS on cancer cell cytotoxicity for three different GBM cell lines, i.e., U251, LN229 and U87, at exactly the same plasma treatment conditions. This should allow us to draw conclusions on the anti-cancer capacity of pPBS, and on the role of the two above-mentioned plasma species in pPBS for killing cancer cells.

First, it is clear from our experiments that varying the operating conditions during plasma treatment leads to different ratios of H_2O_2 and NO_2^- concentrations in pPBS, which can be important to consider when we know

	NO ₂ ⁻	H ₂ O ₂	U251	LN229	U87
Gap ↗	↘	↘	↘	↘	↘
Gas flow rate ↗	↘	↗	↗	↗	↗
Effect of plasma treatment time: ± linear?	✓	✓	✓	✓	×
Discharges at the liquid surface	↗ × 2	↗ × 4	↗ ≥ × 2	↗ ≥ × 2	↗ ≥ × 2
Stability of pPBS?	✓	✓	✓	✓	✓
Stability of pPBS + medium?	✓	?	×	×	×

Table 5. Summary. The effect of gap, gas flow rate, plasma treatment time, the occurrence of discharges at the liquid surface, and the stability of pPBS and pPBS with medium, on the concentrations of NO₂⁻ and H₂O₂ in pPBS and on the anti-cancer capacity of pPBS for three different cancer cell lines.

the exact role of individual species on cancer cell cytotoxicity and on their selectivity towards normal cells. To explain the generation processes of both H₂O₂ and NO₂⁻, we used a 0D chemical kinetics model. We found that the H₂O₂ concentration is mostly determined by the time needed for OH radicals to reach the liquid (affected by the gap and flow rate). Indeed, this determines whether the OH radicals will recombine into H₂O₂ (at high OH_{liquid} concentrations) or whether they will be consumed by N-species, forming HNO₂–HNO₃. For the NO₂⁻ concentration, on the other hand, our model predicts that (i) by increasing the flow rate, fewer ambient air species are able to diffuse into the plasma plume, thereby lowering the NO₂⁻ concentration, and (ii) by increasing the gap, more O₃ will be generated, which will consume NO₂⁻, hence again lowering the NO₂⁻ concentration.

Furthermore, our experiments revealed that H₂O₂ is a major contributor to cancer cell cytotoxicity while NO₂⁻ plays a minor role, but other reactive species should also play a role in the anti-cancer activity of pPBS. A synergistic effect between H₂O₂ and NO₂⁻ is found for the U87 cell line, but not for the U251 and LN229 cell lines. This fact, in combination with the trends of NO₂⁻ and H₂O₂ concentration and percentage cell cytotoxicity as a function of different parameters, seems to suggest that H₂O₂ is a more important species for the anti-cancer capacity of pPBS than NO₂⁻, although assessing the concentrations of other plasma species, such as NO₃⁻ and ONOO⁻, in pPBS is required in the future to draw final conclusions on the role of various plasma species in the anti-cancer capacity of pPBS. In this context, it is worth to mention that we also tried to measure the O₃ concentration in pPBS, but that no signal could be detected. This suggests that O₃, while it may be brought into the solution with the plasma gas, will probably rapidly disappear from it (likely back into the gas phase). Thus we may conclude that O₃ might not play an important role in the anti-cancer capacity of pPBS.

Table 5 summarizes the results of the effects of all plasma treatment parameters on the NO₂⁻ and H₂O₂ concentrations in pPBS, and on the cell cytotoxicity of the three different cancer cell lines. Increasing the gap results in lower concentrations of both NO₂⁻ and H₂O₂, as well as reduced cell cytotoxicity. This is logical because the plasma species are not so efficiently transferred into the liquid, which is less effective for killing the cancer cells. Increasing the gas flow rate leads to a drop in the NO₂⁻ concentration, because this species will not be formed so efficiently in the gas phase, as the N₂ and O₂ from the surrounding air come less in contact with the reactive plasma species. On the other hand, a higher gas flow rate yields a higher H₂O₂ concentration and also more cell cytotoxicity. This indicates that the anti-cancer capacity of pPBS is more related to the presence of H₂O₂ in the liquid than to the presence of NO₂⁻. Increasing the plasma treatment time yields a more or less linear increase in both the NO₂⁻ and H₂O₂ concentrations in pPBS, and in the percentage cell cytotoxicity, except for the U87 cell line, although it is a bit dangerous to draw final conclusions on the linearity for the cancer cell cytotoxicity, based on only a few data points.

We also investigated the effect of the occurrence of discharges at the liquid surface on the NO₂⁻ and H₂O₂ concentrations in pPBS and on the cancer cell cytotoxicity, and observed that these discharges have a significant influence, yielding a factor 2 and 4 higher NO₂⁻ and H₂O₂ concentration in the liquid, as well as at least a factor 2 higher anti-cancer capacity of the pPBS. Indeed, these discharges allow electrons to reach the liquid and to produce more reactive species in the liquid due to electron impact reactions. This is important to realize as a small variation of the gap (in our case between 10 and 15 mm) results in either the presence or absence of discharges at the liquid surface.

Finally, the fact that pPBS is stable at room temperature for at least 2 hours, while pPBS with medium is not, indicates that pPBS might be a more suitable storage medium for practical applications in a clinical setting than PAM, which is until now most often applied.

References

- Schlegel, J., Köritzer, J. & Boxhammer, V. Plasma in cancer treatment. *Clinical Plasma Medicine* **1**, 2–7 (2013).
- Barekzi, N. & Laroussi, M. Effects of low temperature plasmas on cancer cells. *Plasma Process. Polym.* **10**, 1039–1050 (2013).
- Ratovitski, E. A. *et al.* Anti-cancer therapies of 21st century: novel approach to treat human cancers using cold atmospheric plasma. *Plasma Process. Polym.* **11**, 1128–1137 (2014).
- Lu, X. *et al.* Reactive species in non-equilibrium atmospheric-pressure plasmas: generation, transport, and biological effects. *Phys. Rep.* **630**, 1–84 (2016).
- Kim, S. J., Chung, T. H., Bae, S. H. & Leem, S. H. Induction of apoptosis in human breast cancer cells by a pulsed atmospheric pressure plasma jet. *Appl. Phys. Lett.* **97**, 023702 (2010).
- Wang, M. *et al.* Cold atmospheric plasma for selectively ablating metastatic breast cancer cells. *PLoS ONE* **8**, e73741 (2013).
- Kim, J. Y. *et al.* Apoptosis of lung carcinoma cells induced by a flexible optical fiber-based cold microplasma. *Biosens. Bioelectron.* **28**, 333–338 (2011).

8. Kim, S. J., Joh, H. M. & Chung, T. H. Production of intracellular reactive oxygen species and change of cell viability induced by atmospheric pressure plasma in normal and cancer cells. *Appl. Phys. Lett.* **103**, 153705 (2013).
9. Kumar, N. *et al.* The action of microsecond-pulsed plasma-activated media on the inactivation of human lung cancer cells. *J. Phys D: Appl. Phys.* **49**, 115401 (2016).
10. Barekzi, N. & Laroussi, M. Dose-dependent killing of leukemia cells by low-temperature plasma. *J. Phys. D: Appl. Phys.* **45**, 422002 (2012).
11. Partecke, L. I. *et al.* Tissue tolerable plasma (TTP) induces apoptosis in pancreatic cells *in vitro* and *in vivo*. *BMC Cancer* **12**, 473 (2012).
12. Zhang, X., Li, M., Zhou, R., Feng, K. & Yang, S. Ablation of liver cancer cells *in vitro* by a plasma needle. *Appl. Phys. Lett.* **93**, 021502 (2008).
13. Zhao, S. *et al.* Atmospheric pressure room temperature plasma jets facilitate oxidative and nitrate stress and lead to endoplasmic reticulum stress dependent apoptosis in HepG2 cells. *PLoS ONE*, **8**, e73665 (2013).
14. Duan, J., Lu, X. & He, G. The selective effect of plasma activated medium in an *in vitro* co-culture of liver cancer and normal cells. *J. Appl. Phys.* **121**, 013302 (2017).
15. Tanaka, H. *et al.* Plasma-activated medium selectively kills glioblastoma brain tumor cells by down-regulating a survival signaling molecule, AKT kinase. *Plasma Med.* **1**, 265–277 (2011).
16. Vandamme, M. *et al.* ROS implication in a new antitumor strategy based on non-thermal plasma. *Int. J. Cancer*. **130**, 2185–2194 (2012).
17. Yan, D. *et al.* The role of aquaporins in the anti-glioblastoma capacity of the cold plasma-stimulated medium. *J. Phys D: Appl. Phys.* **50**, 055401 (2017).
18. Vermeylen, S. *et al.* Cold atmospheric plasma treatment of melanoma and glioblastoma cancer cells. *Plasma Process. Polym.* **13**, 1195–1205 (2016).
19. Ahn, H. J. *et al.* Atmospheric-pressure plasma jet induces apoptosis involving mitochondria via generation of free radicals. *PLoS ONE* **6**, e28154 (2011).
20. Ishaq, M. *et al.* Atmospheric gas plasma-induced ROS production activates TNF-ASK1 pathway for the induction of melanoma cancer cell apoptosis. *Mol. Biol. Cell* **25**, 1523–1531 (2014).
21. Fridman, G. *et al.* Floating electrode dielectric barrier discharge plasma in air promoting apoptotic behavior in melanoma skin cancer cell lines. *Plasma Chem. Plasma Process* **27**, 163–176 (2007).
22. Kim, G. C. *et al.* Air plasma coupled with antibody-conjugated nanoparticles: a new weapon against cancer. *J. Phys. D: Appl. Phys.* **42**, 032005 (2009).
23. Lee, H. J. *et al.* Degradation of adhesion molecules of G361 melanoma cells by a non-thermal atmospheric pressure microplasma. *New J. Phys.* **11**, 115026 (2009).
24. Trachootham, D., Alexandre, J. & Huang, P. Targeting cancer cells by ROS-mediated mechanisms: a radical therapeutic approach? *Nat. Rev. Drug Discov.* **8**, 579–591 (2009).
25. Yan, D. *et al.* Toward understanding the selective anticancer capacity of cold atmospheric plasma—a model based on aquaporins (Review). *Biointerphases* **10**, 040801 (2015).
26. Van der Paal, J., Neyts, E. C., Verlackt, C. C. W. & Bogaerts, A. Effect of lipid peroxidation on membrane permeability of cancer and normal cells subjected to oxidative stress. *Chem. Sci.* **7**, 489–498 (2016).
27. Van der Paal, J., Verheyen, C., Neyts, E. C. & Bogaerts, A. Hampering effect of cholesterol on the permeation of reactive oxygen species through phospholipids bilayer: possible explanation for plasma cancer selectivity. *Sci. Reports* **7**, 39526 (2017).
28. Sato, T., Yokoyama, M. & Johkura, K. A key inactivation factor of HeLa cell viability by a plasma flow. *J. Phys. D: Appl. Phys.* **44**, 372001 (2011).
29. Canal, C. *et al.* Plasma-induced selectivity in bone cancer cells death. *Free Radic. Biol. Med.* **110**, 72–80 (2017).
30. Yan, D. *et al.* Controlling plasma stimulated media in cancer treatment application. *Appl. Phys. Lett.* **105**, 224101 (2014).
31. Yan, D. *et al.* Principles of using cold atmospheric plasma stimulated media for cancer treatment. *Sci. Rep.* **5**, 18339 (2015).
32. Yan, D., Nourmohammadi, N., Talbot, A., Sherman, J. H. & Keidar, M. The strong anti-glioblastoma capacity of the plasma-stimulated lysine-rich medium. *J. Phys D: Appl. Phys.* **49**, 274001 (2016).
33. Adachi, T. *et al.* Plasma-activated medium induces A549 cell injury via a spiral apoptotic cascade involving the mitochondrial-nuclear network. *Free Radic. Biol. Med.* **79**, 28–44 (2015).
34. Yan, D. *et al.* Stabilizing the cold plasma-stimulated medium by regulating medium's composition. *Sci. Rep.* **6**, 26016 (2016).
35. Wende, K. *et al.* Identification of the biologically active liquid chemistry induced by a nonthermal atmospheric pressure plasma jet. *Biointerphases* **10**, 029518 (2015).
36. Boehm, D., Heslin, C., Cullen, P. J. & Bourke, P. Cytotoxic and mutagenic potential of solutions exposed to cold atmospheric plasma. *Sci. Rep.* **6**, 21464 (2016).
37. Yan, D. *et al.* The specific vulnerabilities of cancer cells to the cold atmospheric plasma-stimulated solutions. *Sci. Rep.* **7**, 4479 (2017).
38. Girard, P.-M. *et al.* Synergistic effect of H₂O₂ and NO₂ in cell death induced by cold atmospheric He plasma. *Sci. Rep.* **6**, 29098 (2016).
39. Tanaka, H. *et al.* Non-thermal atmospheric pressure plasma activates lactate in Ringer's solution for anti-tumor effect. *Sci. Rep.* **6**, 36282 (2016).
40. Bruggeman, P. J. *et al.* Plasma-liquid interactions: a review and roadmap. *Plasma Sources Sci. Technol.* **25**, 053002 (2016).
41. Winter, J. *et al.* Tracking plasma generated H₂O₂ from gas into liquid phase and revealing its dominant impact on human skin cells. *J. Phys. D: Appl. Phys.* **47**, 285401 (2014).
42. Takamatsu, T. *et al.* Investigation of reactive species using various gas plasmas. *RSC Adv.* **4**, 39901 (2014).
43. Gorbanev, Y., O'Connell, D. & Chechik, V. Non-thermal plasma in contact with water: the origin of species. *Chem. Eur. J.* **22**, 3496–3505 (2016).
44. Tresp, H., Hammer, M. U., Winter, J., Weltmann, K.-D. & Reuter, S. Quantitative detection of plasma-generated radicals in liquids by electron paramagnetic resonance spectroscopy. *J. Phys. D: Appl. Phys.* **46**, 435401 (2013).
45. Yokoyama, M., Johkura, K. & Sato, T. Gene expression responses of HeLa cells to chemical species generated by an atmospheric plasma flow. *Biochem. Biophys. Res. Commun.* **450**, 1266–1271 (2014).
46. Mohades, S., Laroussi, M., Sears, J., Barekzi, N. & Razavi, H. Evaluation of the effects of a plasma activated medium on cancer cells. *Phys. Plasmas* **22**, 122001 (2015).
47. Judée, F. *et al.* Short and long time effects of low temperature plasma activated media on 3D multicellular tumor spheroids. *Sci. Rep.* **6**, 21421 (2016).
48. Adachi, T. *et al.* Iron stimulates plasma-activated medium-induced A549 cell injury. *Sci. Rep.* **6**, 20928 (2016).
49. Kurake, N. *et al.* Cell survival of glioblastoma grown in medium containing hydrogen peroxide and/or nitrite, or in plasma-activated medium. *Arch. Biochem. Biophys.* **605**, 102–108 (2016).
50. Agnihotri, S. *et al.* Glioblastoma, a brief review of history, molecular genetics, animal models and novel therapeutic strategies. *Arch. Immunol. Ther. Exp.* **61**, 25–41 (2013).
51. Louis, D. N. *et al.* The 2007 WHO classification of tumours of the central nervous system. *Acta Neuropathol.* **114**, 97–109 (2007).
52. Stupp, R. *et al.* Effect of radiotherapy with concomitant and adjuvant temozolomide versus radiotherapy alone on survival in glioblastoma in a randomised phase III study: 5-year analysis of the EORTC-NCIC trial. *Lancet Oncol.* **10**, 459–466 (2009).

53. Bekeschus, S., Schmidt, A., Weltmann, K.-D. & von Woedtke, T. The plasma jet kINPen – a powerful tool for wound healing. *Clin. Plasma Med.* **4**, 19–28 (2016).
54. Mann, M. S. *et al.* Introduction to DIN-specification 91315 based on the characterization of the plasma jet kINPen[®] MED. *Clin. Plasma Med.* **4**, 35–45 (2016).
55. Eisenberg, G. M. Colorimetric determination of hydrogen peroxide. *Ind. Eng. Chem. Anal. Ed.* **15**, 327–328 (1943).
56. Lukes, P., Dolezalova, E., Sisrova, I. & Clupek, M. Aqueous-phase chemistry and bactericidal effects from an air discharge plasma in contact with water: evidence for the formation of peroxydinitrite through a pseudo-second-order post-discharge reaction of H₂O₂ and HNO₂. *Plasma Sources Sci. Technol.* **23**, 015019 (2014).
57. Satterfield, C. N. & Bonnell, A. H. Interferences in titanium sulfate method for hydrogen peroxide. *Anal. Chem.* **27**, 1174–1175 (1955).
58. Anbar, M. & Taube, H. Interaction of nitrous acid with hydrogen peroxide and with water. *J. Am. Chem. Soc.* **76**, 6243–6247 (1954).
59. Fox, J. B. Kinetics and mechanisms of the griess reaction. *Anal. Chem.* **51**, 1493–1502 (1979).
60. Vichai, V. & Kirtikara, K. Sulforhodamine B colorimetric assay for cytotoxicity screening. *Nat. Protoc.* **1**, 1112–1116 (2016).
61. Gibicka, L. & Didik, J. Catalytic scavenging of peroxydinitrite by catalase. *J. Inorg. Biochem.* **103**, 1375–1379 (2009).
62. Takeda, S. *et al.* Intraperitoneal administration of plasma-activated medium: proposal of a novel treatment option for peritoneal metastasis from gastric cancer. *Ann. Surg. Oncol.* **24**, 1188–1194 (2017).
63. Mohades, S., Barezki, N., Razavi, H., Marathammathu, V. & Laroussi, M. Temporal evaluation of the anti-tumor efficiency of plasma-activated medium. *Plasma Process. Polym.* **13**, 1206–1211 (2016).

Acknowledgements

We acknowledge financial support from the Fund for Scientific Research (FWO) Flanders (Grant No. 11U5416N), the Research Council of the University of Antwerp and the European Marie Skłodowska-Curie Individual Fellowship “LTPAM” within Horizon2020 (Grant No. 743151). Finally, we would like to thank P. Attri and A. Privat Maldonado for the valuable discussions.

Author Contributions

W.V.B., Y.G. and S.V. designed the experiments. W.V.B. performed the experiments. J.V.d.P. designed and performed the simulations. W.V.B., J.V.d.P. and A.B. wrote the manuscript. All authors reviewed the manuscript.

Additional Information

Supplementary information accompanies this paper at <https://doi.org/10.1038/s41598-017-16758-8>.

Competing Interests: The authors declare that they have no competing interests.

Publisher's note: Springer Nature remains neutral with regard to jurisdictional claims in published maps and institutional affiliations.



Open Access This article is licensed under a Creative Commons Attribution 4.0 International License, which permits use, sharing, adaptation, distribution and reproduction in any medium or format, as long as you give appropriate credit to the original author(s) and the source, provide a link to the Creative Commons license, and indicate if changes were made. The images or other third party material in this article are included in the article's Creative Commons license, unless indicated otherwise in a credit line to the material. If material is not included in the article's Creative Commons license and your intended use is not permitted by statutory regulation or exceeds the permitted use, you will need to obtain permission directly from the copyright holder. To view a copy of this license, visit <http://creativecommons.org/licenses/by/4.0/>.

© The Author(s) 2017

Anti-cancer capacity of plasma-treated PBS: effect of chemical composition on cancer cell cytotoxicity

Wilma Van Boxem^{1,*}, Jonas Van der Paal¹, Yury Gorbanev¹, Steven Vanuytsel^{1,2}, Evelien Smits², Sylvia Dewilde³ and Annemie Bogaerts^{1,*}

¹ Research group PLASMANT, Department of Chemistry, University of Antwerp
Universiteitsplein 1, BE-2610 Wilrijk-Antwerp, Belgium

² Center for Oncological Research (CORE), University of Antwerp
Universiteitsplein 1, BE-2610 Wilrijk-Antwerp, Belgium

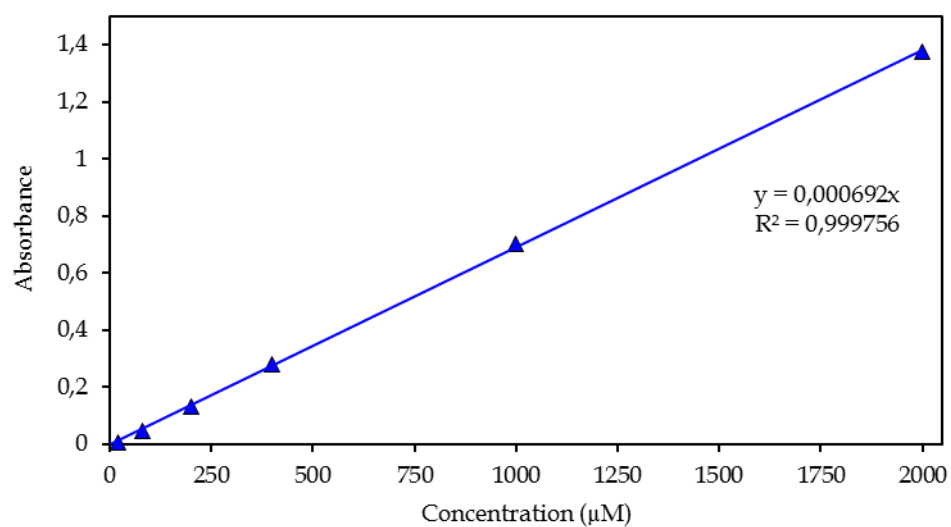
³ Research group PPES, Department of Biomedical Sciences, University of Antwerp
Universiteitsplein 1, BE-2610 Wilrijk-Antwerp, Belgium

* wilma.vanboxem@uantwerpen.be

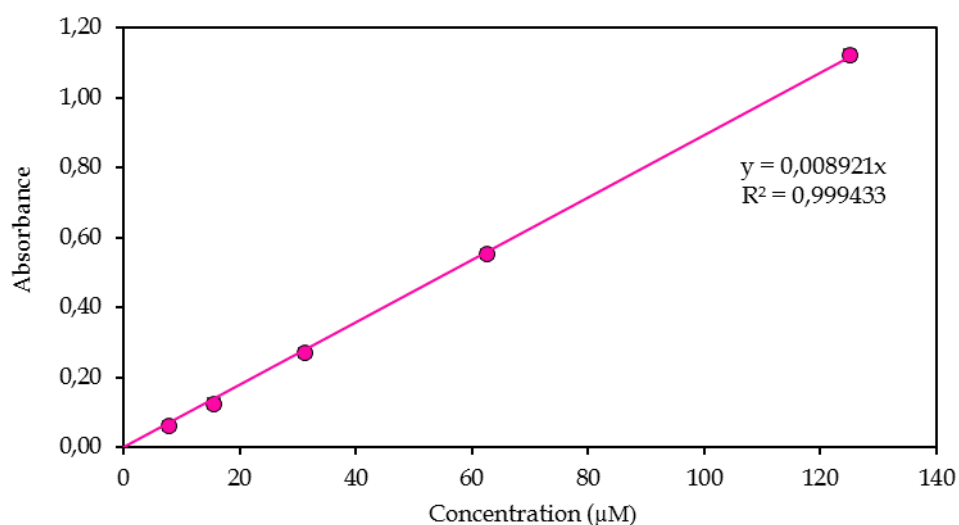
* annemie.bogaerts@uantwerpen.be

Supplementary Information

Calibration curves



Supplementary Figure S1. Calibration curve for measurement of H_2O_2 . Standard solutions of H_2O_2 between 20 and 2000 μM were used to determine the extinction coefficient as $\epsilon = 692 \text{ L mol}^{-1} \text{ cm}^{-1}$.



Supplementary Figure S2. Calibration curve for measurement of NO_2^- . Standard solutions of NO_2^- between 7.8 and 125 μM were used to determine the extinction coefficient as $\epsilon = 8921 \text{ L mol}^{-1} \text{ cm}^{-1}$.

Model Description

Chemical kinetics model

The chemical kinetics model is based on solving a set of conservation equations (1) for all individual species included in the model (see below):

$$\frac{\partial n_s}{\partial t} = \sum_{i=1}^j [(a_{s,i}^R - a_{s,i}^L)R_i] \quad (1)$$

in which n_s is the density of species s (m^{-3}), j the total number of reactions, $a_{s,i}^L$ and $a_{s,i}^R$ the stoichiometric coefficients at the left hand side and right hand side of the reaction and R_i the rate of reaction (in $\text{m}^{-3} \text{s}^{-1}$), given by:

$$R_i = k_i \prod_s n_s^{\alpha_{s,i}} \quad (2)$$

in which k_i is the rate coefficient ($\text{m}^3 \text{s}^{-1}$ or $\text{m}^6 \text{s}^{-1}$ for two-body or three-body reactions, respectively). The rate coefficients of the heavy particle reactions are either constant or dependent on the gas temperature, whereas the rate coefficients of the electron impact reactions depend on the electron temperature T_e or the reduced electric field E/N (i.e., the electric field E divided by the number density of all neutral species N , usually expressed in $\text{Td} = 10^{-21} \text{V m}^2$). The rate coefficients of the electron impact reactions are generally calculated according to the following equation:

$$k_i = \int_{\varepsilon_{th}}^{\infty} \sigma_i(\varepsilon) v(\varepsilon) f(\varepsilon) d\varepsilon \quad (3)$$

with ε the electron energy (usually in eV), ε_{th} the minimum threshold energy needed to induce the reaction, $v(\varepsilon)$ the velocity of the electrons (in m s^{-1}), $\sigma_i(\varepsilon)$ the cross section of collision i (in m^2), and $f(\varepsilon)$ the (normalized) electron energy distribution function (EEDF; in eV^{-1}) calculated using a Boltzmann solver.

In this work we solve the balance equations (1) of all species by means of the ZDPlaskin code, which also has a built-in Boltzmann solver, called BOLSIG+^{S.1}, to calculate the EEDF and the rate coefficients of the electron impact reactions^{S.2} based on a set of cross sections, the plasma composition, the gas temperature and the reduced electric field (E/N). The electric field (E ; in V m^{-1}) is calculated from a given power density, using the so-called local field approximation^{S.3}:

$$E = \sqrt{\frac{P}{\sigma}} \quad (4)$$

with P the input power density (in W m^{-3}) and σ the plasma conductivity ($\text{A V}^{-1} \text{m}^{-1}$). The plasma conductivity is estimated at the beginning of the simulations as^{S.3}:

$$\sigma = \frac{e^2 n_{e,init}}{m_e v_m} \quad (5)$$

with e the elementary charge ($1.6022 \times 10^{-19} \text{C}$), $n_{e,init}$ the initial electron density (in m^{-3}), m_e the electron mass ($9.1094 \times 10^{-31} \text{kg}$) and v_m the collision frequency (in s^{-1}) calculated using BOLSIG+. During the simulation the plasma conductivity is calculated as^{S.3}:

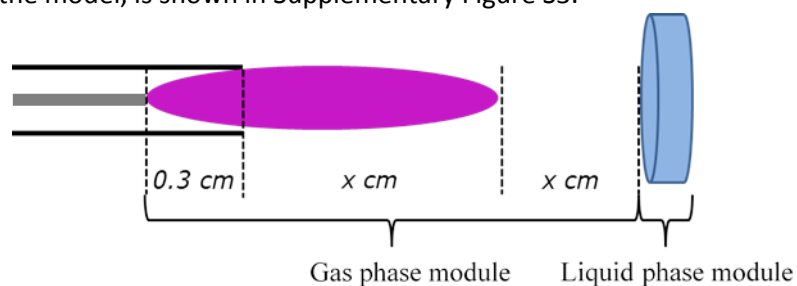
$$\sigma = \frac{e v_d n_e}{(\frac{E}{N})_{prev} n_0} \quad (6)$$

with v_d the electron drift velocity (in m s^{-1}), which is calculated using BOLSIG+ implemented in ZDPlaskin, and $(\frac{E}{N})_{prev}$ the reduced electric field at the previous time step (in V m^2).

Description of the plasma jet in the chemical kinetics model

In the approach of using a chemical kinetics model to simulate the kINPen plasma jet studied in this work, a cylindrical volume element is followed along the jet stream. By doing this, we assume a homogenous plasma along the radial axis (cfr. plug flow reactor). Moreover, we assume that the axial transport of mass and energy due to drift and diffusion is negligible compared to convection. Due to the very high axial flow speed (order of 10^3cm s^{-1}) compared to the radial flow speed this seems acceptable. Upon reaching the liquid substrate, the calculated gas phase densities of all plasma species are used as input for the liquid phase module. In this module, the accumulation of species in the liquid is determined by the diffusion from gas phase species into the liquid, which is based on Henry's law, as well as by the liquid-phase chemistry. This approach, which allows us to investigate the liquid

chemistry using a chemical kinetics model, was introduced by Lietz *et al.*^{5,4} The general plasma jet set-up, assumed in the model, is shown in Supplementary Figure S3.

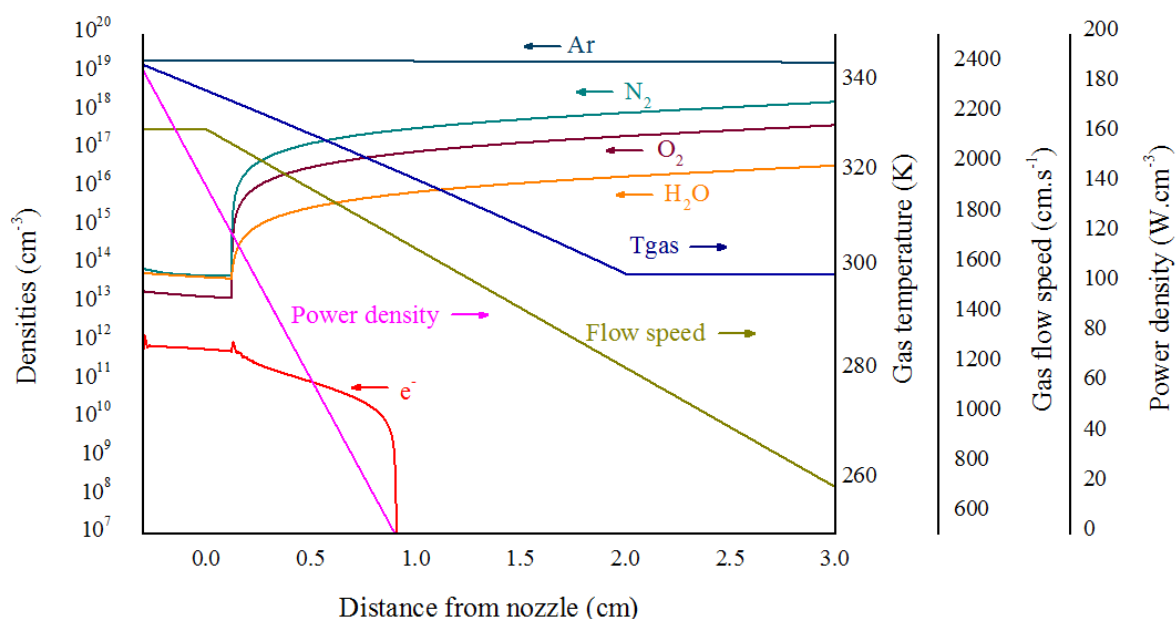


Supplementary Figure S3. Plasma jet set-up used in the chemical kinetics model. The start of the simulation is 3 mm before the nozzle, which is at the tip of the inner electrode (thick gray line). The length of the visible plasma plume (indicated in purple) and the total distance between nozzle and liquid sample (both denoted as x cm) depend on the specific treatment conditions (see Table 1 in the main paper).

Gas phase module

Conceptually, a chemical kinetics model calculates the density of all species as a function of time (see equation 1). However, by assuming a certain velocity profile of the feed gas, this time can be coupled to the position of the volume element along the axis, which allows us to obtain information on the species densities as a function of distance, and thus to investigate different treatment distances, as used in the experiments. An example of the gas flow velocity profile, which decreases along the axis due to gas expansion and obstruction by the relatively stationary surrounding atmosphere, is shown in Supplementary Figure S4, for a gas flow rate of 1 slm. The initial gas flow velocity, at the nozzle, is calculated based on the flow rate of the feed gas and the dimensions of the plasma jet.

Furthermore, as mentioned above, many of the gas phase reaction rate coefficients depend on the gas temperature. This means that a gas temperature profile along the plasma axis is required to calculate the exact rate of all reactions (see Supplementary Figure S4). This temperature profile is based on our experimental measurements.



Supplementary Figure S4. Plasma and gas characteristics as a function of the distance from the nozzle, along the plasma jet axis, for the conditions of a flow rate of 1 slm and a treatment distance of 30 mm. The profiles of the power deposition, gas temperature and humid air densities in argon due to diffusion are fitted to (i) experimental values and (ii) more detailed 2D simulations^{S.5}. The electron density is calculated throughout the simulation. The grey area indicates the interior of the plasma jet, starting from the electrode tip, where the simulation starts. Note that the plasma and gas characteristics at other conditions of flow rate and treatment distance are somewhat different.

Moreover, as the electron impact reactions depend on the EEDF, the reduced electric field is also required. As mentioned above, this reduced field is calculated based on the deposited power density, of which an example profile is also shown in Supplementary Figure S4. The maximum value of the power density is achieved at the tip of the powered electrode. Subsequently, the power density decreases linearly along the plasma axis, reaching zero at the end of the visible plasma plume, which is observed experimentally. This is chosen as the simulation results indicate that the densities of the excited species quickly drop to zero when the power density drops to zero, due to which the visible plasma plume would also be lost. The length of the plasma plume depends on the gas flow rate, based on our experimental observations, i.e., at 1 slm, the plasma plume propagates in general 9 mm into the surrounding atmosphere, whereas at 3 slm, the plasma plume has a length of 12 mm. In the case of 1 slm and a treatment distance of 10 mm, plasma discharges onto the liquid substrate were observed, as mentioned in the main paper. This means that under these conditions, a discharge between two electrodes occurs, (i) the electrode tip from the plasma jet and (ii) the liquid surface. Therefore, we assume the power density profile to rise again slightly upon reaching the liquid surface (i.e. at the end of the gas phase simulation). In all cases, the total deposited power equals 3.5 W, as is the case in the experimental treatments.

Finally, to mimic the mixing of humid air species into the effluent of the plasma jet, these species (O₂, N₂ and H₂O) are added into the effluent, assuming a certain air mixing rate (based on experimental data). The profiles of the ambient air species along the axis are also shown in Supplementary Figure S4. Note that the diffusion of ambient air species only starts after 0.12 cm in the effluent. This is because it will take some time before the ambient air species are able to diffuse up to the plasma axis. The initial densities of O₂, N₂ and H₂O inside the device (grey area in Supplementary Figure S4) originate from the impurities of the feed gas (1, 4 and 3 ppm for O₂, N₂ and H₂O, respectively), which are taken the same as the impurities present in the feed gas used in the experimental work.

The chemistry set of the gas phase reactions used in this study is largely taken from Murakami *et al.*^{S.6} However, to include additional relevant biomedically active species (e.g. H₂O₂, HO₂, HNO₃ or HNO₂), we extended this chemistry set with the reactions describing the behavior of these species, adopted from the chemistry set of Van Gaens and Bogaerts^{S.7}, yielding a total chemistry set of 91 different species and 1390 reactions. All species included in the gas phase are shown in Supplementary Table S1.

Supplementary Table S1. Species taken into account in the chemical kinetics model for the gas phase. The species in bold are also taken into account in the liquid phase.

Ground state neutrals	Excited state neutrals	Charged species
Ar	Ar(⁴ S[³ P ₂]), Ar(⁴ S[³ P ₁]), Ar(⁴ S[³ P ₀]), Ar(⁴ S[¹ P ₁]), Ar(4P)	e ⁻ , Ar ⁺ , Ar ₂ ⁺ , ArH ⁺
N, N ₂	N(² D), N(² P), N _{2, vib(1-4)} , N _{2, rot} , N ₂ (A ³ Σ _u ⁺), N ₂ (a' ¹ Σ _u ⁻)	N ⁺ , N ₂ ⁺ , N ₃ ⁺ , N ₄ ⁺
O, O ₂ , O ₃	O(¹ D), O(¹ S), O _{2, vib(1-5)} , O _{2, rot} , O ₂ (a ¹ Δ _g), O ₂ (b ¹ Σ _g ⁺)	O ⁺ , O ₂ ⁺ , O ₄ ⁺ , O ⁻ , O ₂ ⁻ , O ₃ ⁻
NO, NO ₂ , NO ₃ , N ₂ O, N ₂ O ₃ , N ₂ O ₄ , N ₂ O ₅		NO ⁺ , NO ₂ ⁺ , N ₂ O ⁺ , NO ⁻ , NO ₂ ⁻ , NO ₃ ⁻
H, H ₂ , OH, H ₂ O, HO ₂ , H ₂ O ₂	H [*] , H _{2, vib} , H _{2, rot} , H ₂ [*] , OH(A)	H ⁺ , H ₂ ⁺ , H ₃ ⁺ , OH ⁺ , H ₂ O ⁺ , H ₃ O ⁺ , H ⁻ , OH ⁻ , O ₂ H ₂ O ⁻ , H ₂ O ⁻ , HO ₂ ⁻
NH, HNO, HNO ₂ , HNO ₃ , HNO ₄ , ONOOH		NO ₂ H ₂ O ⁻ , NO ₃ H ₂ O ⁻ , ONOO ⁻

Liquid phase module

To investigate the chemistry occurring in the plasma treated liquid, a second set of species and a separate chemistry set^{S.4} were included in the chemical kinetics model. First, a duplicate solvated species was added for each important gas phase species (e.g. O_{3aq} for O₃). The choice was either based on the final gas phase density of these species or their relevance for the biomedical applications. These aqueous species and the liquid reactions are restricted to the liquid module only (and are thus not taken into account in the gas phase module). The species in these two modules can only interact through the gas-liquid interphase by means of diffusion into or out of the liquid. In general, the densities of the liquid species are given by^{S.4}:

$$\frac{\partial n_s}{\partial t} = \sum_{i=1}^j [(a_{s,i}^R - a_{s,i}^L)R_i] + \frac{D_s n_{s,g}}{\lambda^2} f_l S_{s,l} \frac{V_p}{V_l} - \max \left[0, \frac{D_s (n_{s,l} - h_s n_{s,g}) V_p}{\lambda^2 V_l} \right] \quad (7)$$

in which the first term is similar to the calculation of the gas phase species densities (conservation of mass; see above). The second term represents the diffusion of gas phase species into the liquid. In this term, D_s is the diffusion coefficient of gas phase species s , $n_{s,g}$ is the final gas phase density of species s and λ is the diffusion length of the plasma. Furthermore, f_l is the fraction of the area of the plasma in contact with the liquid and $S_{s,l}$ is the sticking coefficient of species s on the liquid, given by:

$$S_{s,l} = \frac{h_s n_{s,g} - n_{s,l}}{h_s n_{s,g}} \quad (8)$$

in which h_s represents the Henry constant of species s . This sticking coefficient is only used if $n_{s,l}/n_{s,g} < h_s$ and accounts for a diminishing rate of loss of the gas phase species into the liquid as the liquid density approaches its Henry's law equilibrium values. Finally, V_p and V_l represent the volume of the plasma and the liquid, respectively. The third term of equation 7 is only non-zero if the liquid is oversaturated (i.e. if $n_{s,l}/n_{s,g} > h_s$) and represents the flux from the liquid phase into the gas phase. The Henry constants were adopted from Lietz *et al.*^{S.4}, whereas the diffusion coefficients were taken from Verlackt *et al.*^{S.5}. As mentioned before, the reaction chemistry of the liquid phase is taken from Lietz *et al.*^{S.4} and includes in total 35 species and 89 reactions. It is impossible to take into account the transportation of plasma species from the gas-liquid interface into the bulk of the liquid by means of this OD chemical kinetics model, but in reality, the density of the short-lived reactive species, such as OH radicals, will drop

quickly from the interface towards the bulk. We mimic this drop in species densities in our model by decreasing the reaction rate coefficients of the reactions involving these short-lived species with longer-lived species. This approach is based on observations from more detailed 2D fluid simulations carried out in our group, in which short-lived species react mostly at the gas-liquid interface, generating more stable species, which are then rapidly transported towards the bulk of the liquid due to convection.^{S,5}

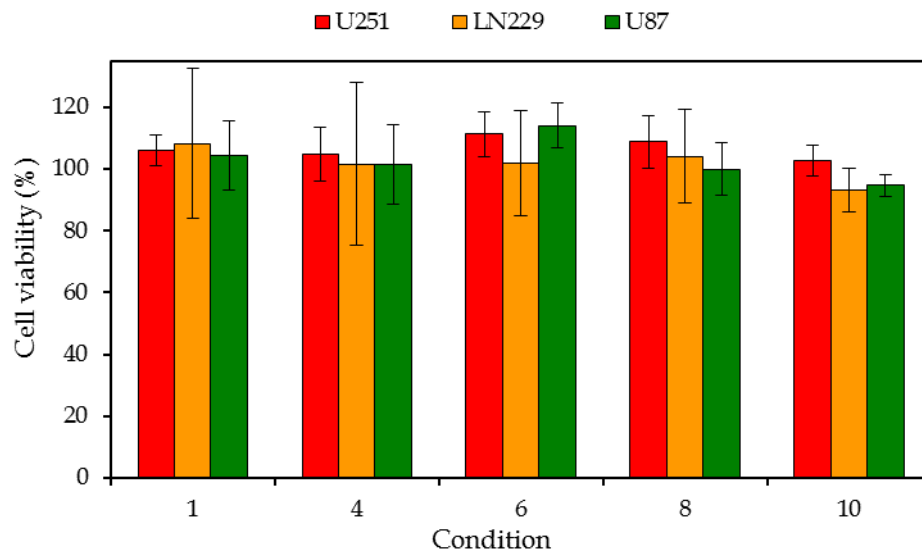
Finally, it is important to mention that the liquid in our model is pure water, with 4.8 ppm O₂ and 8.9 ppm N₂ initially dissolved into it (equilibrium values with air). The experiments were performed in a buffered solution at pH 7.3, so the concentrations of H₃O⁺ and OH⁻ in the liquid were fixed throughout the entire simulation at values which correspond to this pH.

Supplementary Table S2. List of reactions included in the liquid module.

Reaction	Rate coefficient
ONOOH _{aq} + H ₂ O _{aq} → H ₃ O ⁺ _{aq} + ONOO ⁻ _{aq}	5.0x10 ⁻¹⁵
ONOO ⁻ _{aq} + H ₃ O ⁺ _{aq} → H ₂ O _{aq} + ONOOH _{aq}	1.75x10 ⁻⁶
HO _{2aq} + H ₂ O _{aq} → H ₃ O ⁺ _{aq} + O ₂ ⁻ _{aq}	1.43x10 ⁻¹⁷
H ₃ O ⁺ _{aq} + O ₂ ⁻ _{aq} → HO _{2aq} + H ₂ O _{aq}	5.0x10 ⁻¹¹
HNO _{2aq} + H ₂ O _{aq} → H ₃ O ⁺ _{aq} + NO ₂ ⁻ _{aq}	5.0x10 ⁻¹⁵
H ₃ O ⁺ _{aq} + NO ₂ ⁻ _{aq} → HNO _{2aq} + H ₂ O _{aq}	3.9x10 ⁻¹⁰
HNO _{3aq} + H ₂ O _{aq} → H ₃ O ⁺ _{aq} + NO ₃ ⁻ _{aq}	3.0x10 ⁻¹⁸
H ₃ O ⁺ _{aq} + NO ₃ ⁻ _{aq} → HNO _{3aq} + H ₂ O _{aq}	7.0x10 ⁻¹⁶
HO ₂ NO _{2aq} + H ₂ O _{aq} → O ₂ NO ₂ ⁻ _{aq} + H ₃ O ⁺ _{aq}	5.0x10 ⁻¹⁵
O ₂ NO ₂ ⁻ _{aq} + H ₃ O ⁺ _{aq} → HO ₂ NO _{2aq} + H ₂ O _{aq}	1.05x10 ⁻⁷
OH _{aq} + H _{aq} → H ₂ O _{aq}	3.0x10 ⁻¹¹
H ₂ O ⁻ _{aq} + H ₂ O _{aq} → H _{aq} + OH ⁻ _{aq} + H ₂ O _{aq}	3.0x10 ⁻²⁰
H ₂ O ⁻ _{aq} + H _{aq} → H _{2aq} + OH ⁻ _{aq}	4.0x10 ⁻¹¹
H ₂ O ⁻ _{aq} + O _{2aq} → H ₂ O _{aq} + O ₂ ⁻ _{aq}	3.0x10 ⁻¹¹
H ₂ O ⁻ _{aq} + OH _{aq} → H ₂ O _{aq} + OH ⁻ _{aq}	5.0x10 ⁻¹¹
H ₂ O ⁻ _{aq} + H ₂ O _{2aq} → H ₂ O _{aq} + OH ⁻ _{aq} + OH _{aq}	2.0x10 ⁻¹³
H ₂ O ⁻ _{aq} + HO ₂ ⁻ _{aq} → OH ⁻ _{aq} + OH ⁻ _{aq} + OH _{aq}	5.0x10 ⁻¹²
H ₂ O ⁻ _{aq} + H ₂ O ⁻ _{aq} → H _{2aq} + OH ⁻ _{aq} + OH ⁻ _{aq}	1.0x10 ⁻¹¹
H ₃ O ⁺ _{aq} + OH ⁻ _{aq} → H ₂ O _{aq} + H ₂ O _{aq}	5.0x10 ⁻¹⁵
H ₂ O _{aq} + H ₂ O _{aq} → H ₃ O ⁺ _{aq} + OH ⁻ _{aq}	3.02x10 ⁻³²
OH _{aq} + OH _{aq} → H ₂ O _{2aq}	1.7x10 ⁻¹¹
OH _{aq} + H _{2aq} → H _{aq} + H ₂ O _{aq}	6.0x10 ⁻¹⁴
OH _{aq} + HO _{2aq} → O _{2aq} + H ₂ O _{aq}	2.0x10 ⁻¹¹
OH _{aq} + H ₂ O _{2aq} → HO _{2aq} + H ₂ O _{aq}	0.45x10 ⁻¹⁵
OH ⁺ _{aq} O ₂ ⁻ _{aq} → O _{2aq} + OH ⁻ _{aq}	1.5x10 ⁻¹¹
OH _{aq} + HO ₂ ⁻ _{aq} → HO _{2aq} + OH ⁻ _{aq}	1.5x10 ⁻¹¹
OH _{aq} + NO ₂ ⁻ _{aq} → OH ⁻ _{aq} + NO _{2aq}	0.3x10 ⁻¹⁵
OH _{aq} + NO _{aq} → HNO _{2aq}	3.3x10 ⁻¹¹
OH _{aq} + NO _{2aq} → HNO _{3aq}	2.0x10 ⁻¹¹
OH _{aq} + HNO _{3aq} → NO _{3aq} + H ₂ O _{aq}	2.17x10 ⁻¹⁵
OH _{aq} + N ₂ O _{aq} → HNO _{aq} + NO _{aq}	3.8x10 ⁻¹⁷
H _{aq} + H ₂ O _{aq} → H _{2aq} + OH _{aq}	1.5x10 ⁻²¹
H _{aq} + H _{aq} → H _{2aq}	1.5x10 ⁻¹¹
H _{aq} + OH ⁻ _{aq} → H ₂ O ⁻ _{aq}	3.0x10 ⁻¹⁴
H _{aq} + HO _{2aq} → H ₂ O _{2aq}	3.0x10 ⁻¹¹
H _{aq} + H ₂ O _{2aq} → H ₂ O _{aq} + OH _{aq}	1.5x10 ⁻¹⁵
H _{aq} + HNO _{aq} → OH _{aq} + NH _{aq}	2.18x10 ⁻²²

$H_{aq} + OH^-_{aq} \rightarrow E_{aq} + H_2O_{aq}$	2.0×10^{-14}
$H_{aq} + NO_2^-_{aq} \rightarrow NO_{aq} + OH^-_{aq}$	7.5×10^{-15}
$H_{aq} + HNO_{2aq} \rightarrow NO_{aq} + H_2O_{aq}$	3.52×10^{-14}
$H_{2aq} + H_2O_{2aq} \rightarrow H_{aq} + OH_{aq} + H_2O_{aq}$	1.0×10^{-14}
$O_{aq} + H_2O_{aq} \rightarrow OH_{aq} + OH_{aq}$	2.2×10^{-17}
$O_{aq} + O_{2aq} \rightarrow O_{3aq}$	5.0×10^{-12}
$O_{2aq} + H_{aq} \rightarrow HO_{2aq}$	5.0×10^{-11}
$O_2(a^1\Delta_g)_{aq} + H_2O_{aq} \rightarrow O_{2aq} + H_2O_{aq}$	5.0×10^{-15}
$O_2^-_{aq} + HO_{2aq} + H_2O_{aq} \rightarrow O_{2aq} + H_2O_{2aq} + OH^-_{aq}$	2.68×10^{-34}
$O_2^-_{aq} + H_2O_{2aq} \rightarrow O_{2aq} + OH_{aq} + OH^-_{aq}$	2.16×10^{-24}
$O_2^-_{aq} + NO_{aq} \rightarrow NO_3^-_{aq}$	6.0×10^{-12}
$O_{3aq} \rightarrow O_{2aq} + O_{aq}$	3.0×10^{-6}
$O_{3aq} + OH^-_{aq} \rightarrow O_2^-_{aq} + HO_{2aq}$	1.16×10^{-19}
$N_{aq} + N_{aq} \rightarrow N_{2aq}$	5.0×10^{-14}
$N_{aq} + H_2O_{aq} \rightarrow NH_{aq} + OH_{aq}$	6.93×10^{-39}
$NH_{aq} + NO_{aq} \rightarrow N_2O_{aq} + H_{aq}$	1.3×10^{-12}
$NH_{aq} + O_{2aq} \rightarrow HNO_{aq} + O_{aq}$	2.3×10^{-13}
$NO_{aq} + NO_{aq} + O_{2aq} \rightarrow NO_{2aq} + NO_{2aq}$	6.28×10^{-36}
$NO_{aq} + NO_{2aq} + H_2O_{aq} \rightarrow HNO_{2aq} + HNO_{2aq}$	5.55×10^{-34}
$NO_{aq} + HO_{2aq} \rightarrow HNO_{3aq}$	5.33×10^{-12}
$NO_{aq} + HO_{2aq} \rightarrow ONOOH_{aq}$	5.33×10^{-12}
$NO_{aq} + O_2^-_{aq} \rightarrow ONOO^-_{aq}$	7.14×10^{-12}
$2 NO_{2aq} + 2 H_2O_{aq} \rightarrow H_3O^+_{aq} + NO_3^-_{aq} + HNO_{2aq}$	1.26×10^{-56}
$2 NO_{2aq} + 3 H_2O_{aq} \rightarrow 2 H_3O^+_{aq} + NO_3^-_{aq} + NO_2^-_{aq}$	1.30×10^{-79}
$NO_{2aq} + OH_{aq} \rightarrow ONOOH_{aq}$	1.99×10^{-11}
$NO_{2aq} + H_{aq} \rightarrow HNO_{2aq}$	1.67×10^{-11}
$NO_2^-_{aq} + O_{3aq} \rightarrow NO_3^-_{aq} + O_{2aq}$	5.48×10^{-16}
$NO_{3aq} + H_2O_{aq} \rightarrow HNO_{3aq} + OH_{aq}$	4.8×10^{-14}
$N_2O_{3aq} + H_2O_{aq} \rightarrow HNO_{2aq} + HNO_{2aq}$	1.93×10^{-17}
$N_2O_{4aq} + H_2O_{aq} \rightarrow HNO_{2aq} + HNO_{3aq}$	1.33×10^{-18}
$N_2O_5^+_{aq} + H_2O_{aq} \rightarrow NO_{2aq} + NO_{3aq} + H_2O_{aq}$	1.4×10^{-19}
$N_2O_5_{aq} + H_2O_{aq} \rightarrow HNO_{3aq} + HNO_{3aq}$	2.0×10^{-21}
$N_2O_5_{aq} + H_2O_{aq} \rightarrow ONOOH_{aq} + ONOOH_{aq}$	2.0×10^{-21}
$H_2O_{2aq} + NO_2^-_{aq} + H_3O^+_{aq} \rightarrow ONOOH_{aq} + H_2O_{aq} + H_2O_{aq}$	3.04×10^{-39}
$ONOOH_{aq} + H_2O_{aq} \rightarrow H_3O^+_{aq} + NO_3^-_{aq}$	2.9×10^{-23}
$ONOOH_{aq} + H_2O_{aq} \rightarrow OH_{aq} + NO_{2aq} + H_2O_{aq}$	1.24×10^{-23}
$HNO_{aq} + O_{2aq} \rightarrow HO_{2aq} + NO_{aq}$	8.01×10^{-21}
$HNO_{aq} + O_{3aq} \rightarrow O_{2aq} + HNO_{2aq}$	9.61×10^{-15}
$HNO_{aq} + OH_{aq} \rightarrow H_2O_{aq} + NO_{aq}$	8.00×10^{-11}
$O_2NO_2^-_{aq} \rightarrow NO_2^-_{aq} + O_{2aq}$	1.0×10^0
$HO_2NO_{2aq} + HNO_{2aq} \rightarrow HNO_{3aq} + HNO_{3aq}$	1.99×10^{-20}
$HO_2NO_{2aq} \rightarrow HNO_{2aq} + O_{2aq}$	7.0×10^{-4}
$HO_2NO_{2aq} \rightarrow HO_{2aq} + NO_{2aq}$	4.6×10^{-3}
$e_{aq} + H_2O_{aq} \rightarrow H_{aq} + OH^-_{aq}$	3.04×10^{-20}
$e_{aq} + E_{aq} + 2 H_2O_{aq} \rightarrow H_{2aq} + 2 OH^-_{aq}$	4.096×10^{-55}
$e_{aq} + H_{aq} + H_2O_{aq} \rightarrow H_{2aq} + OH^-_{aq}$	6.4×10^{-32}
$e_{aq} + OH_{aq} \rightarrow OH^-_{aq}$	4.80×10^{-11}
$e_{aq} + H_3O^+_{aq} \rightarrow H_{aq} + H_2O_{aq}$	3.68×10^{-11}
$e_{aq} + H_2O_{2aq} \rightarrow OH_{aq} + OH^-_{aq}$	1.76×10^{-11}
$e_{aq} + HO_2^-_{aq} + H_2O_{aq} \rightarrow OH_{aq} + 2 OH^-_{aq}$	8.96×10^{-33}
$e_{aq} + O_{2aq} \rightarrow O_2^-_{aq}$	3.04×10^{-11}
$e_{aq} + H_2O_{aq} \rightarrow H_2O^-_{aq}$	5.0×10^{-15}

Catalase experiments



Supplementary Figure S5. Catalase experiments. Effect of adding catalase (400 U mL^{-1}) to pPBS on the cancer cell viability for three different GBM cell lines (U251, LN229, U87). The treatment conditions are listed in Table 1. The percentages are plotted as the mean of at least three repetitions, and the error bars indicate the standard deviations of the mean. No cell cytotoxicity is observed upon addition of catalase, indicating that H_2O_2 plays an important role in the cancer cell cytotoxicity of pPBS, although it might not be the only important species, as catalase might also be able to scavenge other RONS.

References

- S.1 Hagelaar, G. J. M. & Pitchford, L.C. Solving the Boltzmann equation to obtain electron transport coefficients and rate coefficients for fluid models. *Plasma Sources Sci. Technol.* **14**, 722-733 (2005).
- S.2 Pancheshnyi, S., Eismann, B., Hagelaar, G. J. M. & Pitchford, L. C. ZDPlasKin: a new tool for plasmachemical simulations. (2008).
- S.3 Lieberman, M. A. & Lichtenberg, A. J. Principles of Plasma Discharges and Materials Processing (second edition) (Wiley-Interscience, 2005).
- S.4 Lietz, A. M. & Kushner, M. J. Air plasma treatment of liquid covered tissue: long timescale chemistry. *J. Phys. D.: Appl. Phys.* **49**, 425204 (2016).
- S.5 Verlackt, C. W. To be submitted.
- S.6 Murakami, T., Niemi, K., Gans, T. & O'Connell, D. Chemical kinetics and reactive species in atmospheric pressure helium-oxygen plasmas with humid-air impurities. *Plasma Sources Sci. Technol.* **22**, 15003 (2013).
- S.7 Van Gaens, W. & Bogaerts, A. Kinetic modelling for an atmospheric pressure argon plasma jet in humid air. *J. Phys. D.: Appl. Phys.* **46**, 275201 (2013).